Next-to-next-to-leading order event generation for VH production with $H \to b\bar{b}$ decay

Silvia Zanoli,[a] **Mauro Chiesa,**[b] **Emanuele Re,**[c,d] **Marius Wiesemann**[a] **and Giulia Zanderighi**[a,e]

[a]*Max-Planck-Institut für Physik,*
Föhringer Ring 6, 80805 München, Germany

[b]*Dipartimento di Fisica, Università di Pavia, and INFN, Sezione di Pavia,*
Via A. Bassi 6, 27100 Pavia, Italy

[c]*INFN, Sezione di Milano - Bicocca, and Università di Milano - Bicocca,*
Piazza della Scienza 3, 20126 Milano, Italy

[d]*LAPTh, Université Grenoble Alpes, Université Savoie Mont Blanc, CNRS,*
74940 Annecy, France

[e]*Physik-Department, Technische Universität München,*
James-Franck-Strasse 1, 85748 Garching, Germany

E-mail: zanoli@mpp.mpg.de, mauro.chiesa@unipv.it,
emanuele.re@mib.infn.it, marius.wiesemann@mpp.mpg.de,
zanderi@mpp.mpg.de

ABSTRACT: We consider the Higgsstrahlung process in hadronic collisions and present the computation of next-to-next-to-leading order predictions matched to parton showers for both production and $H \to b\bar{b}$ decay employing the MiNNLO$_{\rm PS}$ method. We present predictions for ZH and $W^{\pm}H$ production including spin correlations and off-shell effects by calculating the full processes $pp \to \ell^+\ell^- H \to \ell^+\ell^- b\bar{b}$, $pp \to \nu_\ell \bar{\nu}_\ell H \to \nu_\ell \bar{\nu}_\ell b\bar{b}$ and $pp \to \ell^\pm \nu_\ell H \to \ell^\pm \nu_\ell b\bar{b}$ in the narrow-width approximation for the Higgs boson. For the $W^{\pm}H$ process, NNLO+PS accuracy in production and decay is achieved for the first time. Our calculations are validated against earlier simulations in the NNLOPS approach that includes NNLO corrections via multi-differential reweighting. The new MiNNLO$_{\rm PS}$ generators for these processes, which evaluate NNLO corrections on-the-fly in the event generation, will supersede those earlier calculations. Our predictions are in good agreement with recent measurements of the Higgsstrahlung cross sections.

KEYWORDS: Higgs Production, Higher-Order Perturbative Calculations, Parton Shower, Resummation

ARXIV EPRINT: 2112.04168

Contents

1 Introduction

The Higgs boson is a unique particle in the Standard Model of Particle Physics (SM). Although it interacts with all massive particles, which obtain their masses precisely through their interaction with the Higgs field, only with the high-energy proton-proton collisions of the Large Hadron Collider (LHC) the Higgs boson could be discovered due it its relatively large mass of 125 GeV. The discovery in 2012 was based on 5 fb^{-1} of data collected at 7 and 8 TeV [1, 2]. A discovery in this early stage of the LHC was possible since the Higgs boson has a sufficiently large branching fraction to photons and Z bosons, which lead to experimentally very clean signatures with an excellent mass resolution. Since the discovery studying the properties of the observed scalar resonance has been one of the cornerstones of the rich physics programme at the LHC. In particular, the Higgs sector provides a window to new-physics phenomena that could for instance affect the Higgs couplings. With all Higgs properties appearing to be SM-like thus far and without any other clear signs of physics beyond the SM (BSM), precision tests of the Higgs sector have become a valuable path towards the observation of new physics.

Higgs-boson production at the LHC proceeds predominantly through gluon fusion and is induced by a top-quark loop, while the Higgs decay to bottom quarks ($H \rightarrow b\bar{b}$) has the largest branching ratio. Other Higgs-production modes are suppressed by roughly one order of magnitude or more with respect to gluon fusion, but they are indispensable in the study of the Higgs properties to determine as many of the Higgs couplings as possible. For instance, the associated production of a Higgs boson and a vector boson (VH production or "Higgsstrahlung") or vector-boson fusion (VBF) provide access to Higgs couplings to vector bosons, increasing the sensitivity to those couplings in addition to the Higgs decay modes to vector bosons. Even more importantly, the $H \rightarrow b\bar{b}$ decay, which provides direct access to the bottom Yukawa coupling, could only be observed [3, 4] by exploiting the VH production mode with a boosted Higgs boson. In fact, it had been thought for a long time that Higgsstrahlung would not be accessible at the LHC until it was proposed to consider VH events where the Higgs boson has large transverse momentum (i.e. it is boosted) and to apply substructure techniques to identify the bottom quarks and reconstruct the Higgs boson [5]. This renders the accurate modeling of both VH production and the $H \rightarrow b\bar{b}$ decay at the level of fully exclusive events indispensable. While this was already crucial for the experiments to observe this decay mode, it will become even more critical for an accurate determination of the bottom Yukawa coupling in the future.

A remarkable progress in next-to-next-to-leading order (NNLO) QCD calculations for SM processes has been made in the past years, with all $2 \rightarrow 2$ colour-singlet scattering processes computed at this accuracy [6–39], and even first NNLO calculations for genuine $2 \rightarrow 3$ processes emerging in the recent past [40–43]. The Higgsstrahlung process is actually much simpler from a computational point of view: as far as QCD corrections are concerned the calculation corresponds to an extension of the Drell-Yan (DY) process in which the Higgs boson is emitted from the vector boson. Indeed, the inclusive NNLO cross section was computed almost twenty years ago [44–46], and about ten years later fully differential NNLO calculations appeared [6–9, 47–49]. Part of the NNLO corrections to ZH production is the loop-induced gluon-fusion (gg) process, which is mediated by a top-quark loop, while other contributions mediated by a top-quark loop have been shown to be relatively small [45] and are thus often neglected in differential calculations. In fact, the effectively only leading-order (LO) accurate loop-induced gg process dominates the theoretical uncertainties in ZH analyses, which calls for the inclusion of NLO corrections to $gg \rightarrow ZH$ production, especially since first approximations suggested that these are quite large [50–53]. Recently, substantial progress was made in the calculation of the relevant two-loop amplitude to (on-shell) $gg \rightarrow ZH$ production [54–56], which eventually led to the first calculation at NLO QCD in a small mass expansion [53]. Strategies to isolate the $gg \rightarrow ZH$ component in experimental analyses have been suggested in ref. [57]. The analytic resummation of logarithms at threshold and due to a jet veto in VH production have been considered in refs. [51, 58–60]. Recently, also $W^{\pm}H$ production in association with a jet was calculated at NNLO accuracy in QCD [61]. As far as NLO electroweak (EW) corrections are concerned, they have been available for a while [62–64].

Since VH measurements exploit a particularly differential strategy, requiring a boosted Higgs and substructure techniques, as discussed before, it is mandatory to combine state-

of-the-art higher-order calculations with full-fledged event simulations through a parton shower (PS) Monte Carlo generator. NLO QCD corrections matched to parton showers are available as a merged calculation for $VH + 0, 1$-jet production within POWHEG [65] using the MiNLO′ method [66, 67]. Similarly, both NLO QCD and EW corrections were simultaneously matched to a parton shower in a merged VH+0,1-jet calculation in ref. [68]. Predictions at LO+PS for $gg \to ZH$ can be easily obtained with several tools, including with POWHEG-BOX [65]. Merged predictions at LO, up to $gg \to ZH + 1$-jet, have been considered in refs. [69, 70], and a study on how different approximations compare has also been performed in ref. [71]. The effects from anomalous couplings in VH production have been considered within POWHEG in ref. [72]. In recent years, a great effort has been devoted to the matching of NNLO QCD calculations and parton showers (NNLO+PS), and essentially four different methods have been introduced: the NNLOPS method [73] based on reweighting MiNLO′ events [67], the UNNLOPS method [74, 75], the GENEVA method [76], and, most recently, the MiNNLO$_{PS}$ approach [77, 78]. At first these methods have been applied to the simplest colour singlet processes, namely Higgs-boson production [73, 75, 79] and Drell Yan [74, 80, 81]. Especially in the NNLOPS, MiNNLO$_{PS}$ and GENEVA approaches a variety of colour-singlet production processes are now available at NNLO+PS, including ZH [82, 83], $W^{\pm}H$ [83, 84], $\gamma\gamma$ [85], $Z\gamma$ [86, 87], $W^{\pm}\gamma$ [88], ZZ [89, 90] and $W^{+}W^{-}$ [91, 92] production. Very recently, also the NNLO+PS matching for the very first production process with coloured particles in the initial and final state has been achieved in ref. [93], which extents the MiNNLO$_{PS}$ method to top-quark pair production.

Similarly important in this context is an accurate and fully exclusive description of the $H \to b\bar{b}$ decay. The total decay rate for massless bottom quarks is known to N^{4}LO QCD by now [94–102]. Electroweak corrections were computed in refs. [103–106]. We refer to refs. [107, 108] for a review of calculations for the inclusive $H \to b\bar{b}$ branching ratio. Fully differential calculations are available at fixed-order through NLO QCD for massive bottom quarks since a long time [109–112]. NNLO QCD predictions have been first computed for massless bottom quarks [8, 113–115], and the corresponding results retaining massive bottom quarks were presented in refs. [116–119]. Recently, even the N^{3}LO corrections were calculated in the massless approach [120, 121]. The effect of top-quark loops have been studied in refs. [122, 123]. A complete calculation at NLO QCD in the SM Effective Field Theory (SMEFT) was presented in ref. [124], while anomalous couplings between the vector bosons in the production of the VH final state, including the $H \to b\bar{b}$ decay, were considered at NNLO QCD in ref. [125]. As far as Monte Carlo predictions are concerned, the simulation of $H \to b\bar{b}$ decay events has been achieved at NNLO+PS in refs. [126–128].

In this paper, we present a fully exclusive simulation of ZH and $W^{\pm}H$ production with $H \to b\bar{b}$ decay in the MiNNLO$_{PS}$ framework. Both production and decay events are simulated at NNLO+PS accuracy and consistently combined to obtain accurate predictions for the $\ell^{+}\ell^{-}b\bar{b}$, $\nu_{\ell}\bar{\nu}_{\ell}b\bar{b}$ and $\ell^{\pm}\nu_{\ell}b\bar{b}$ final states, including off-shell effects and spin correlations of the vector bosons and treating the Higgs boson in the narrow-width approximation. NNLO+PS accuracy for the $pp \to \nu_{\ell}\bar{\nu}_{\ell}H \to \nu_{\ell}\bar{\nu}_{\ell}b\bar{b}$ and $pp \to \ell^{\pm}\nu_{\ell}H \to \ell^{\pm}\nu_{\ell}b\bar{b}$ processes is achieved for the first time. Our implementation has been done both within POWHEG-BOX-V2 [129] and within POWHEG-BOX-RES [130], and the ensuing results are completely

compatible within numerical uncertainties. For the $\ell^+\ell^- b\bar{b}$ final state our MiNNLO$_{\rm PS}$ predictions are compared against the NNLOPS results of ref. [126], while for $\ell^\pm\nu_\ell H$ production we validate our calculation against the NNLOPS results presented in ref. [84] for on-shell Higgs bosons. The new MiNNLO$_{\rm PS}$ implementation shall supersede those NNLOPS implementations in the future within the Powheg-Box framework [129]. Finally, we present a complete study of NNLO+PS events for both ZH and $W^\pm H$ production with $H \to b\bar{b}$ decay, finding agreement with a recent LHC measurement from the ATLAS collaboration [131].

This manuscript is organized as follows: in section 2 we introduce our calculation by discussing the processes (section 2.1), sketching the MiNNLO$_{\rm PS}$ method (section 2.2), describing our practical implementation (section 2.3) and recalling the combination of production and decay events (section 2.4). An extensive validation of our MiNNLO$_{\rm PS}$ generator is presented in section 3 against NNLOPS prediction for $W^\pm H$ production without decay (section 3.1) and for ZH production with $H \to b\bar{b}$ decay (section 3.2). In section 4 we present new results for both ZH and $W^\pm H$ production including the $H \to b\bar{b}$ decay: after introducing the setup (section 4.1), we discuss inclusive and fiducial cross sections (section 4.2), distributions in the fiducial phase space (section 4.3), the effect of different clustering algorithms in the definition of bottom-quark jets (section 4.4), and compare against data in (section 4.5). We conclude in section 5. While in the main text we focus on results for W^+H and ZH production, in appendix A we present results for W^-H production.

2 Outline of the calculation

2.1 Description of the processes

We consider the processes

$$pp \to ZH \to \ell^+\ell^- H, \qquad pp \to ZH \to \nu_\ell\bar{\nu}_\ell H \quad \text{and} \quad pp \to W^\pm H \to \ell^\pm\nu_\ell H, \qquad (2.1)$$

for massless leptons $\ell \in \{e, \mu, \tau\}$, where by ν_ℓ we indicate generally a neutrino or anti-neutrino, including the decay mode

$$H \to b\bar{b}. \qquad (2.2)$$

Both production and decay events are generated with NNLO accuracy within the MiNNLO$_{\rm PS}$ framework, introduced in the next section. Their combination is then consistently matched with the Pythia8 [132] parton shower, achieving full-fledged hadron-level NNLO+PS events for the $\ell^+\ell^- b\bar{b}$ and $\ell^\pm\nu_\ell b\bar{b}$ final states, with the only approximation that the interference between the final-state bottom quarks and the initial-state partons vanishes. Indeed, such interference is strongly suppressed because of the small Higgs width and enters only at second order in the strong coupling constant, since the resonant Higgs boson is a colour singlet. Off-shell effects of the intermediate bosons as well as spin correlations of the vector boson are fully taken into account, while the Higgs decay is included in the narrow-width approximation. For ZH production we have implemented both the $Z \to \ell^+\ell^-$ and the
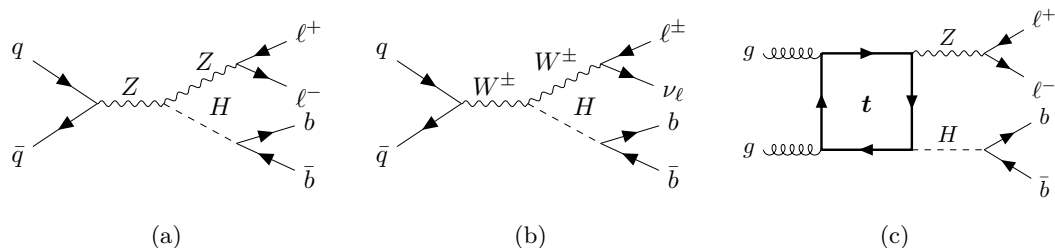
Figure 1. Sample Feynman diagrams for VH production in the $H \to b\bar{b}$ decay channel with (a,c) $V = Z$ and $Z \to \ell^+\ell^-$ and (b) $V = W^\pm$ and $W^\pm \to \ell^\pm\nu_\ell$, where by ν_ℓ we indicate generally a neutrino or anti-neutrino. Panels (a) and (b) are tree-level diagrams in the quark-annihilation ($q\bar{q}$) channel at LO, while panel (c) shows a loop-induced diagram in the gluon-fusion (gg) channel entering at NNLO QCD.

$Z \to \nu_\ell\bar{\nu}_\ell$ decay modes, but, without loss of generality, we focus on the decay to charged leptons throughout this paper. For simplicity, we will refer to the $\ell^+\ell^-b\bar{b}$ and $\ell^\pm\nu_\ell b\bar{b}$ final states as ZH and $W^\pm H$ production in the following.

Sample LO diagrams of the two processes are shown in figure 1 (a) and (b). They are $q\bar{q}$-initiated with an s-channel vector boson emitting a Higgs boson and subsequent decays of the two bosons. Figure 1 (c) shows a diagram for the loop-induced process in the gg channel that due to charge conservation exists only for ZH, but not for $W^\pm H$ production. This process enters the ZH cross section at $\mathcal{O}(\alpha_s^2)$ and is therefore a NNLO contribution relative to the $q\bar{q}$-initiated process. Its dominant contribution proceeds via a top-quark loop, since all other quark loops are suppressed by their respective Yukawa couplings to the Higgs boson. In this work, we focus on the accurate simulation of the $q\bar{q}$-initiated processes. The loop-induced gg process can be computed completely independently at LO+PS and added to the $q\bar{q}$-initiated cross section. We only include the loop-induced gg contribution when presenting integrated cross sections in section 4.2 and when comparing to data in section 4.5. In fact, we would like to stress that very recently the $gg \to ZH$ two-loop amplitude for an on-shell Z boson has been calculated [54–56], which will enable NLO+PS predictions for the loop-induced gg process in the near future (with the approximation of the Z boson being on-shell in the two-loop contribution). Apart from the best predictions for the $q\bar{q}$-initiated ZH production presented here, this calculation will be crucial to reduce the theoretical uncertainties in the experimental analyses of boosted ZH production at the LHC.

We note that there are other contributions to both $W^\pm H$ and ZH production that are mediated by a closed top-quark loop radiating the Higgs boson, which were calculated in ref. [45]. We adopt the approximation that the virtual diagrams denoted as V_I and V_II in ref. [45] are neglected in our calculation, while the real contributions R_I and R_II, where the latter only contributes to ZH production, are included. In order to facilitate the comparison to previous results we have excluded those contributions to $W^\pm H$ production, but included them for ZH production, as discussed below. We recall that the contribution of the $R_\text{I/II}$ and $V_\text{I/II}$ terms to the total cross section is positive. Both $R_\text{I/II}$ and $V_\text{I/II}$ contribute to about 0.6%, giving a total positive correction of about 1.2% with respect to the total $q\bar{q}$-initiated NNLO result obtained neglecting these terms.

2.2 MiNNLO$_{\text{PS}}$ method

Our calculation of VH production at NNLO+PS relies on the MiNNLO$_{\text{PS}}$ method, which was formulated and applied to $2 \to 1$ processes in refs. [77, 78] and later extended to generic colour-singlet processes in ref. [86] and to heavy-quark pair production in ref. [93]. The interested reader is referred to those publications for details, while here we only sketch the main ideas behind the MiNNLO$_{\text{PS}}$ procedure in a simplified notation.

The MiNNLO$_{\text{PS}}$ method that formulates a matching of NNLO corrections with a parton shower for a system F of colour-singlet particles proceeds essentially in three steps: in Step I, a POWHEG calculation [129, 133–135] generates F in association with one light parton at NLO inclusively over the second radiation. In Step II, an appropriate Sudakov form factor and higher-order corrections are applied such that the simulation remains finite in the unresolved limit of the light partons and becomes NNLO accurate for inclusive F production. Step III involves both the exclusive generation of the second radiated parton (accounted for inclusively in Step I) through the POWHEG Sudakov and the generation of subsequent emissions through the parton shower. Since all emissions are correctly ordered in p_T (when using p_T-ordered showers) and the Sudakov in Step II matches the leading logarithms generated by the parton shower, the MiNNLO$_{\text{PS}}$ method preserves the (leading logarithmic) accuracy of the parton shower.

We write the fully differential MiNNLO$_{\text{PS}}$ cross section symbolically as

$$
\begin{aligned}
d\sigma_{\text{F}}^{\text{MiNNLO}_{\text{PS}}} &= d\Phi_{\text{FJ}} \, \bar{B}^{\text{MiNNLO}_{\text{PS}}} \times \left\{ \Delta_{\text{pwg}}(\Lambda_{\text{pwg}}) + d\Phi_{\text{rad}} \Delta_{\text{pwg}}(p_{T,\text{rad}}) \frac{R_{\text{FJ}}}{B_{\text{FJ}}} \right\}, \\
\bar{B}^{\text{MiNNLO}_{\text{PS}}} &\sim e^{-S} \left\{ d\sigma_{\text{FJ}}^{(1)}\left(1 + S^{(1)}\right) + d\sigma_{\text{FJ}}^{(2)} + \left(D - D^{(1)} - D^{(2)} \right) \times F^{\text{corr}} \right\},
\end{aligned}
\tag{2.3}
$$

which corresponds to a POWHEG calculation for F plus one light parton (FJ), but including NNLO accuracy for F production through a modification of the $\bar{B}$ function. Indeed, Δ_{pwg} is the standard POWHEG Sudakov form factor with a default cutoff of $\Lambda_{\text{pwg}} = 0.89 \, \text{GeV}$, Φ_{rad} and $p_{\text{T,rad}}$ are phase space and transverse momentum of the second radiation, respectively, and B_{FJ} and R_{FJ} denote the squared tree-level matrix elements for FJ and FJJ production, respectively, while Φ_{FJ} is the FJ phase space. In the second line $d\sigma_{\text{FJ}}^{(1,2)}$ are the first- and second-order term in the α_s expansion of the differential FJ cross section, while e^{-S} denotes the Sudakov form factor in the transverse momentum of F (p_{T}), with $S^{(1)}$ being the first term in the expansion of the exponent. Renormalization and factorization scales are evaluated as $\mu_{\text{R}} \sim \mu_{\text{F}} \sim p_{\text{T}}$ in MiNNLO$_{\text{PS}}$ and NNLO accuracy is achieved by the last term in the $\bar{B}$ function, which is of order $\alpha_s^3(p_{\text{T}})$ and adds the relevant (singular) contributions [77], while regular contributions at this order are subleading. The function D is derived from the following formula that determines the relevant singular terms in p_{T}

$$
d\sigma_{\text{F}}^{\text{res}} = \frac{d}{dp_{\text{T}}} \left\{ e^{-S} \mathcal{L} \right\} = e^{-S} \underbrace{\left\{ -S' \mathcal{L} + \mathcal{L}' \right\}}_{\equiv D},
\tag{2.4}
$$

which can be obtained by suitably manipulating a p_{T} resummation formula, as explained in section 4 of ref. [77]. $\mathcal{L}$ is the luminosity factor up to NNLO, including the convolution of

the collinear coefficient functions with the parton distribution functions (PDFs) and the squared hard-virtual matrix elements for F production.

Instead of truncating eq. (2.3) at the third order, i.e. evaluating $\left(D - D^{(1)} - D^{(2)}\right) = D^{(3)} + \mathcal{O}(\alpha_s^4)$, as originally done in ref. [77], we keep all terms of $\mathcal{O}(\alpha_s^4)$ and higher, as suggested in ref. [78], in order to preserve the total derivative in eq. (2.4). Finally, the factor F^{corr} in eq. (2.3) ensures that the Born-like NNLO corrections are consistently included in the FJ POWHEG events by spreading them in FJ phase space.

2.3 Practical implementation

We have implemented MiNNLO$_{\text{PS}}$ generators for VH production both in the POWHEG-BOX-V2 [129] and the POWHEG-BOX-RES [130] framework. Both calculations yield fully compatible results within numerical uncertainties. Our POWHEG-BOX-V2 implementation uses the VH+jet generators developed in ref. [65], which were already used in the former NNLOPS calculations of refs. [82, 84]. It then includes NNLO QCD corrections to VH production by exploiting the original implementation of the MiNNLO$_{\text{PS}}$ method for Drell-Yan production of refs. [77, 78], which is suitable since the respective two-loop corrections for VH production correspond to those of the Drell-Yan (DY) process with the Higgs boson being emitted from the vector boson. Our MiNNLO$_{\text{PS}}$ VH generators in POWHEG-BOX-RES, on the other hand, are based on the VH+jet implementation of ref. [68]. The VH+jet generators have then been upgraded to include NNLO QCD accuracy for VH production through the general MiNNLO$_{\text{PS}}$ implementation for colour-singlet production developed for POWHEG-BOX-RES in ref. [86].

As far as the physical amplitudes are concerned, both calculations exploit the same results, documented in refs. [65, 68]. The tree-level real and double-real matrix elements (i.e. for VH+1,2-jet production) are obtained using the automated interface [136] between POWHEG-BOX and MADGRAPH V4 [137]. The VH+jet one-loop amplitude is taken from the analytic calculation of ref. [138]. The one-loop and two-loop amplitudes have been obtained by applying the form-factor correction to the quark vertex function (equivalent to Drell-Yan production) to the Born amplitude. We note that the VH+jet generator of ref. [68] in POWHEG-BOX-RES in principle also allows us to use OPENLOOPS [139–141] for the evaluation of the relevant amplitudes, but we have not made use of that feature. Note that, as discussed before, our VH MiNNLO$_{\text{PS}}$ generators include the R_{I} and R_{II} real contributions, first calculated in ref. [45], while we neglect the V_{I} and V_{II} virtual amplitudes, which contribute below one percent.

The calculation of D in eq. (2.4), which is the central ingredient to include the NNLO QCD corrections through MiNNLO$_{\text{PS}}$, involves the evaluation of several convolutions with the parton distribution functions (PDFs), which are performed through HOPPET [142]. Moreover, the collinear coefficient functions require the computation of polylogarithms, for which we employ the HPLOG package [143].

For the calculation of the decay of the Higgs boson to bottom quarks at NNLO+PS we follow closely the procedure of ref. [126] using the NNLOPS method. Thus, pure $H \to b\bar{b}$ events are generated, such that the inclusive $H \to b\bar{b}$ decay width is NNLO QCD accurate

and observables involving an extra jet are NLO QCD accurate. While for the generation of decay events we could also apply the MiNNLO$_{PS}$ method, we stick to the NNLOPS approach based on including NNLO corrections through an a-posteriori reweighting. This is because in the present case the reweighting is completely straightforward as one needs to reweight to one single number, i.e. to the NNLO decay width of the Higgs boson to bottom quarks. All details about the reweighting are given in section 2.2 of ref. [126]. In particular, we follow the procedure and settings recommended there, i.e. we use the three-jet resolution variable in the Cambridge algorithm (with $y_{3,\text{pow}} = 2$ and $y_{3\text{ref}} = e^{-4}$) to smoothly turn off the reweighting of events accompanied by hard radiation, which are already NLO accurate. All relevant amplitudes have been computed in ref. [114].

Finally, we report the most relevant non-standard settings that we have used in this paper. To turn off spurios higher-order logarithmic terms at large transverse momenta we use a modified logarithm for $p_{\text{T}} > m_{VH}/2$, where m_{VH} is the invariant mass of the Higgs and vector-boson system, which smoothly vanishes at $p_{\text{T}} = m_{VH}$, as introduced in ref. [93]. The hard scale in the logarithm is consistently changed to $m_{VH}/2$ as explained in ref. [144]. At small transverse momenta, we use the standard MiNNLO$_{PS}$ scale setting given in eq. (14) of ref. [78] with $Q_0 = 0\,\text{GeV}$. We regularize the Landau singularity by freezing the strong coupling and the PDFs for scales below $0.8\,\text{GeV}$. Furthermore, we activate the option `largeptscales 1` to set the scales entering the cross section at large transverse momenta [78]. We turn on the POWHEG-BOX option `doublefsr 1`, which was introduced and discussed in detail in ref. [145]. In our interface to the parton-shower we have kept all settings to the standard ones, in particular for the recoil scheme.

2.4 Combining VH production and $H \to b\bar{b}$ decay at NNLO+PS

In order to combine VH production at NNLO+PS with the decay of the Higgs boson to bottom quarks at NNLO+PS, we follow the procedure outlined in ref. [126], which we summarize here. First, $\ell^+\ell^- H$ and $\ell^\pm \nu_\ell H$ production events as well as $H \to b\bar{b}$ decay events are generated, using the calculations outlined in the previous section.

Once available production and decay events are merged following a two-step procedure. First, one replaces, in each production event, the Higgs boson with the decay products of a Higgs boson in a decay event. This procedure is explained in all detail in section 3.1 of ref. [126]. Note that decay events are generated on-shell, while we include the Higgs width in the production events. The procedure performs a rescaling of the decay event in such a way that momentum is conserved exactly but small off-shell effects suppressed by Γ_H/m_H are neglected. Second, the weights of the combined events are set using the production and decay weights. In particular, when multiple weights are present (e.g. to probe scale variations) all possible combinations are included in the final event file. More precisely, the combined weight (w_{full}) of a production event with weight w_{prod} and a decay event with weight w_{dec} is given by

$$w_{\text{full}} = w_{\text{proc}} \cdot \text{Br}_{H \to b\bar{b}} \cdot \frac{w_{\text{dec}}}{\Gamma_{H \to b\bar{b}}}, \tag{2.5}$$

where $\text{Br}_{H \to b\bar{b}}$ is the branching ratio of the Higgs boson to bottom quarks, which is treated as an input, while $\Gamma_{H \to b\bar{b}}$ is the $H \to b\bar{b}$ decay width, which is computed from the decay

events. Accordingly, the last factor in eq. (2.5) integrates to one exactly if one is fully inclusive over the Higgs decay products. This implies that regardless of the accuracy of the last factor (MiNLO′ vs. MiNNLO_PS) the integrated inclusive cross section will be exactly equal to the cross section obtained from the production events times the branching ratio of the Higgs boson to bottom quarks. Similarly, the precise value of the bottom Yukawa coupling used in the Higgs decay cancels out exactly in the ratio of the last factor in eq. (2.5), since we evaluate the Yukawa coupling at a fixed scale m_H.

In order to match the final events to a parton shower one needs to take into account that the starting scale of the shower for production and decay is different. In our combined event file we store the starting scale (`scalup`) of the production stage, while, when interfacing to the shower we recompute on-the-fly the veto scale for the decay (`scalup_dec`) using the decay kinematics, as explained in section 3.2 of ref. [126].

In order to respect the radiation bound coming from the production stage we simply use the `scalup` variable stored in the combined event files, as usually done when interfacing POWHEG with PYTHIA. In order to constrain shower radiation off the decay products, we implement a vetoed shower, i.e. we first allow PYTHIA to generate emissions off the Higgs decay products in all available phase space and, once the shower is completed, we check the hardness of the splittings that were generated in the decays. To do so, we go through all splittings that originated from the Higgs decay products generated by POWHEG and, for each, we compute the corresponding hardness using

$$t = 2\, p_{\rm rad} \cdot p_{\rm em}\, \frac{E_{\rm rad}}{E_{\rm em}}\,, \tag{2.6}$$

where $E_{\rm rad}$ ($E_{\rm em}$) and $p_{\rm rad}$ ($p_{\rm em}$) are the energy and momentum of the radiating (emitted) particle, respectively. If for each of these splittings the hardness is smaller than `scalup_dec`, we accept the showered event, otherwise we reject it and we attempt to shower the event again, until the above requirement is fulfilled. After 1000 shower attempts, we reject the event.

Finally, we note that when interfacing to the shower, we make sure that the automatic matrix element corrections to the decay of the parton shower program are switched off, since they are already included with better accuracy in our combined events.

3 Validation against NNLOPS results

VH production at NNLO+PS has already been calculated with the NNLOPS method, which combines the original MiNLO′ approach [67] with a reweighting procedure fully differential in the Born phase space to include the NNLO corrections. While such reweighting constitutes a substantial technical obstacle and requires an additional handling of the generated MiNLO′ events to include NNLO accuracy a posteriori, the physical results are sound. Precisely the complications related to the reweighting are solved by the newer MiNNLO_PS method, which includes the NNLO corrections directly during the generation of the events. NNLOPS results are available so far for WH production without [84] and for ZH production with $H \rightarrow b\bar{b}$ decay [126]. It is therefore very useful to validate our MiNNLO_PS calculation by comparing to those predictions, which will be done in the following. We will show that

MiNNLO_PS and NNLOPS results are fully compatible, so that our new MiNNLO_PS VH generators supersede the previous NNLOPS ones.

3.1 $W^\pm H$ production

We start by considering $W^\pm H$ production keeping the Higgs boson stable, and we compare our MiNNLO_PS predictions against the results of ref. [84]. Since only results for $W^+ H$ are presented in ref. [84] we consider only this case.

We consider proton-proton collisions at the LHC with a center of mass energy of $\sqrt{s} = 13\,\text{TeV}$ and present predictions for the process $pp \to e^+ \nu_e H$. The input parameters are identical to the ones in ref. [84]. In particular, we use the NNLO set of the MMHT2014nnlo68cl parton densities corresponding to a value of $\alpha_s(m_Z) = 0.118$, and we set $m_W = 80.399\,\text{GeV}$, $\Gamma_W = 2.085\,\text{GeV}$ and $m_H = 125.0\,\text{GeV}$. Furthermore we set $\alpha_{EM} = 1/132.3489$ and $\sin^2\theta_W = 0.2226$. The Higgs boson is considered to be on-shell and, in order to compare with ref. [84], contributions where the Higgs boson is radiated off a heavy quark loop are neglected. As already mentioned, these contributions have been shown to be of the order of 1% (see e.g. section I.5.2.c of ref. [146]). The central renormalization and factorization scales are set following the MiNNLO_PS procedure. The perturbative uncertainties are obtained from a 7-point scale variation, i.e. by varying μ_R and μ_F around the central scale by a factor of two with the constraint $1/2 \leq \mu_R/\mu_F \leq 2$. The phase-space definition is fully inclusive, without any fiducial cuts applied.

The total cross sections are $96.72(4)^{+1.9\%}_{-0.6\%}$ fb for MiNNLO_PS and $96.69(3)^{+1.3\%}_{-1.3\%}$ fb for NNLOPS. Thus they agree at the sub-permille level, which is even within the numerical errors and far below the scale uncertainties. There is a small difference in scale uncertainties, which are of the same size, but slightly asymmetric in the case of MiNNLO_PS. This is a consequence of the different settings of perturbative scales and the treatment of terms beyond accuracy in the two calculations, and it is therefore not unexpected.

Figure 2 compares MiNNLO_PS and NNLOPS results at the level of Les Houches events (LHEs) for various differential distributions. In particular, the Higgs rapidity (y_H) and transverse momentum ($p_{T,H}$), the rapidity (y_{W^+}) and the transverse momentum (p_{T,W^+}) of the W^+ boson, as well as the rapidity of the positron (η_e) and the transverse momentum of the $W^+ H$ system (p_{T,W^+H}) are shown. For all rapidity distributions the central predictions are in excellent agreement between MiNNLO_PS and NNLOPS at the level of $\sim 1\%$, up to statistical fluctuations in the tails. As already observed for the total cross section, some slight differences in the scale-uncertainty bands are visible. Also for the transverse-momentum spectra of the Higgs and W^+ boson we find decent agreement between MiNNLO_PS and NNLOPS. The central predictions differ by less than 1-2%, except for some statistical fluctuations. Finally, the differences in the transverse-momentum spectrum of the $W^+ H$ system are slightly larger, reaching up to 3-4%. However, this distribution is effectively only NLO accurate at $p_{T,W^+H} \gg 0$ and subject to matching ambiguities at intermediate p_{T,W^+H} values, which is indicated also by the enlarged uncertainty bands. Indeed, any difference is fully covered by the scale variations. While the two NNLO+PS methods have the same nominal accuracy, the difference in the size of the uncertainty band of the p_{T,W^+H} distributions in the region $30 \lesssim p_{T,W^+H} \lesssim 90\,\text{GeV}$ can be attributed to the fact that the two
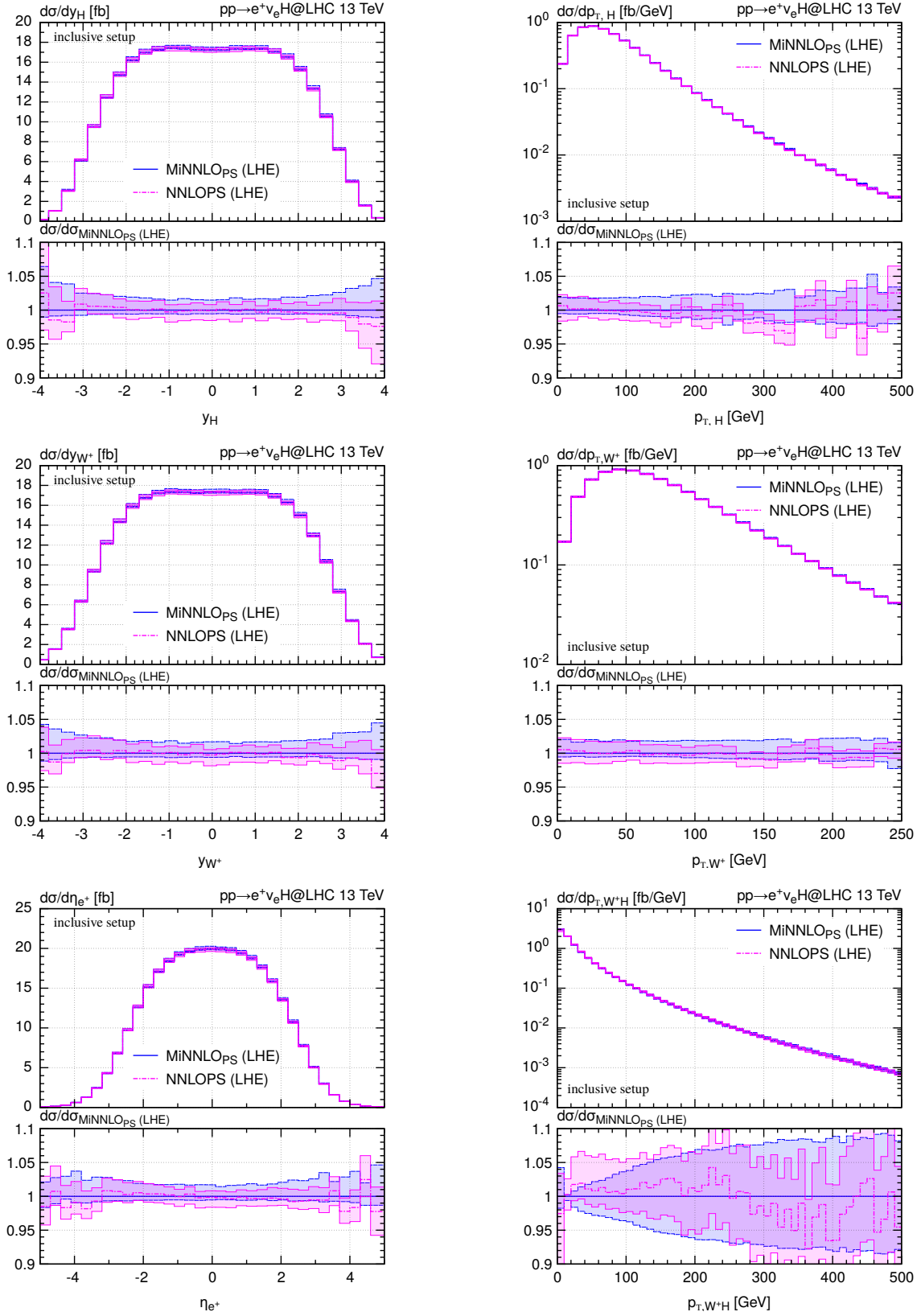
Figure 2. Comparison of MiNNLO$_{PS}$ and NNLOPS predictions for $e^+\nu_e H$ production.

fiducial cuts for $pp \to ZH \to e^+e^- b\bar{b}$
$p_{\mathrm{T},e} > 7\,\mathrm{GeV}$, $p_{\mathrm{T},e_1} > 27\,\mathrm{GeV}$, $|\eta_e| < 2.5$
$81\,\mathrm{GeV} < m_{e^+e^-} < 101\,\mathrm{GeV}$
≥ 2 b-jets (flavour-k_T [147], R=0.4)
$p_{\mathrm{T},b\text{-jet}} > 27\,\mathrm{GeV}$, $|\eta_{b\text{-jet}}| < 2.5$

Table 1. Fiducial cuts for $e^+e^- b\bar{b}$ production from ref. [126].

NNLO+PS methods differ in how the two-loop NNLO corrections are distributed on the p_{T,W^+H} spectrum (i.e. through the use of modified logarithms in MiNNLO$_{\mathrm{PS}}$ and through a p_{T}-dependent multi-differential rescaling in NNLOPS). In particular, as already noticed in ref. [77], the shape of the MiNNLO$_{\mathrm{PS}}$ uncertainty band more closely resembles that of a resummed result matched to a fixed-order prediction.

We have considered many other observables, and we found the same level of agreement for all of them. In conclusion, with agreement typically at the level of $1-2\%$ and at most at the level of a few percent, all within scale variations, the MiNNLO$_{\mathrm{PS}}$ and NNLOPS calculations provide remarkably compatible results, and both calculations can be considered to be equivalent, up to small subleading corrections.

3.2 ZH production with $H \to b\bar{b}$ decay

The situation for ZH production is very similar. First of all, the inclusive cross sections obtained with the new implementation for the production stage (i.e. before including the $H \to b\bar{b}$ decay and without fiducial cuts) have been thoroughly validated against the completely independent fixed-order calculation implemented in MCFM. We find an agreement at the sub-percent level for the inclusive cross section: the central values are $26.567(1)\,\mathrm{fb}$ for MCFM, $26.51(1)\,\mathrm{fb}$ for MiNNLO$_{\mathrm{PS}}$ using the Powheg-Box-Res implementation, and $26.63(9)\,\mathrm{fb}$ using the Powheg-Box-V2 one, where the numbers in brackets refer to statistical uncertainties only. Given that scale uncertainties are at the one-percent level, and that the calculations differ by terms beyond accuracy, the agreement is remarkably good.

We continue by comparing MiNNLO$_{\mathrm{PS}}$ predictions to the results of ref. [126], which correspond to the combination of $pp \to e^+e^- H$ production and $H \to b\bar{b}$ decay at NNLO+PS. Our comparison is thus performed for $e^+e^- b\bar{b}$ events at the LHE level. As before, we consider $\sqrt{s} = 13\,\mathrm{TeV}$ proton-proton collisions at the LHC. The input parameters and fiducial cuts are identical to those in ref. [126]. In particular we use the PDF4LHC15_nnlo_mc parton distribution functions, corresponding to a value of $\alpha_s(m_Z) = 0.118$. We set $m_Z = 91.1876\,\mathrm{GeV}$, $\Gamma_Z = 2.4952\,\mathrm{GeV}$, $m_W = 80.398\,\mathrm{GeV}$, $\Gamma_W = 2.141\,\mathrm{GeV}$, $m_H = 125.0\,\mathrm{GeV}$, $\Gamma_H = 4.14\,\mathrm{MeV}$, and $G_F = 1.166387\times10^{-5}\,\mathrm{GeV}^{-2}$. The EW coupling is computed as $\alpha_{EM} = \sqrt{2}G_F m_W^2(1 - m_W^2/m_Z^2)/\pi$ and the mixing angle as $\cos^2\theta_W = m_W^2/m_Z^2$. The branching ratio for $H \to b\bar{b}$ is set to $\mathrm{Br}_{H\to b\bar{b}} = 0.5824$. For the evaluation of heavy-quark loops we use the bottom-quark pole mass $m_b = 4.92\,\mathrm{GeV}$ and the top-quark pole mass
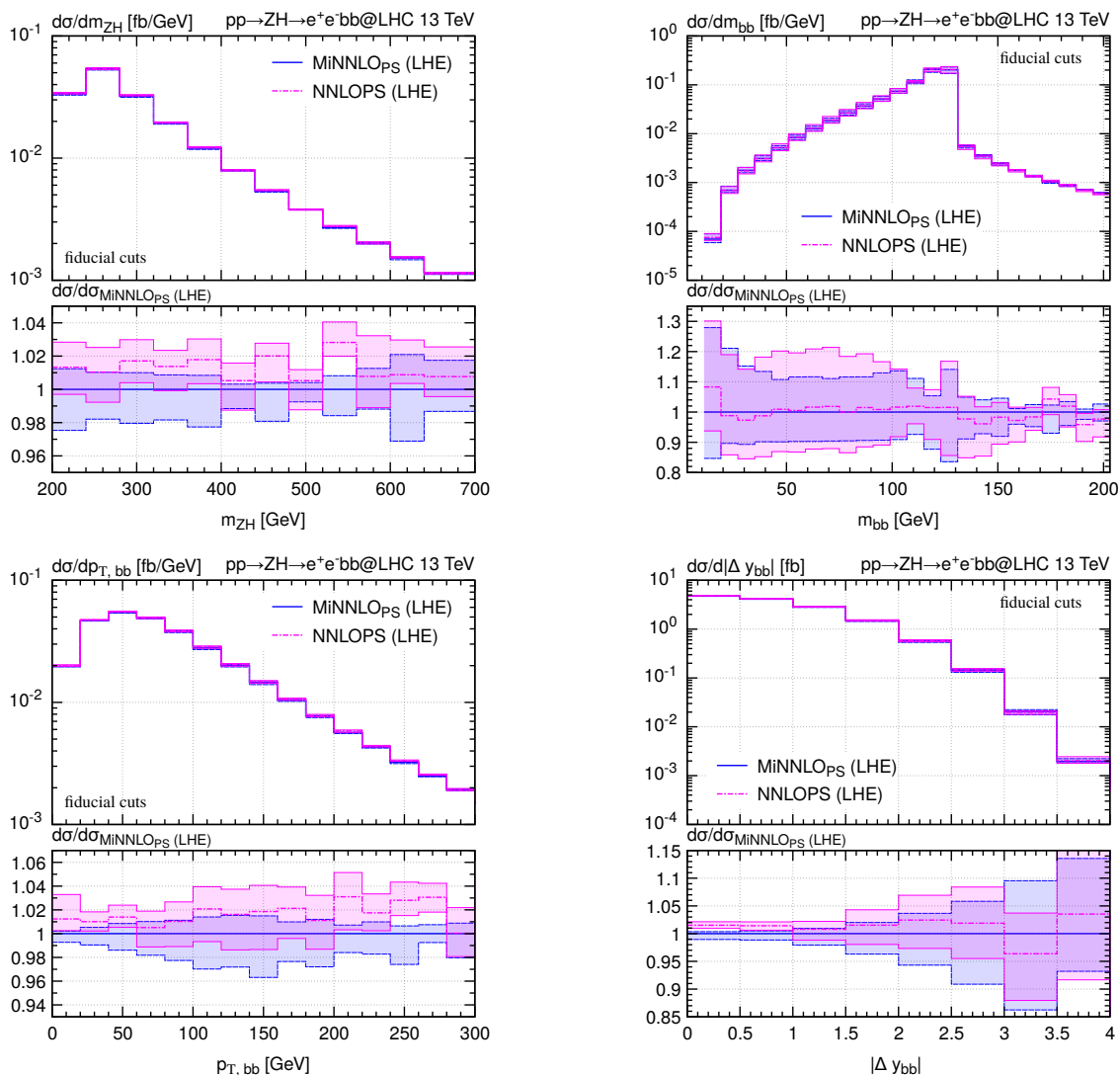
Figure 3. Comparison of MiNNLO$_{PS}$ and NNLOPS predictions for $e^+e^-b\bar{b}$ production with the fiducial cuts quoted in table 1.

$m_t = 173.2\,\text{GeV}$. In the $H \to b\bar{b}$ decay, the bottom Yukawa coupling is evaluated in the $\overline{\text{MS}}$ scheme at a scale equal to the Higgs boson mass m_H with a value of $y_b(m_H) = 1.280$ $\times 10^{-2}$. We would like to stress, however, that given the way production and decay events are combined in eq. (2.5) the precise value of the Yukawa coupling has no impact, as already pointed out in section 2.4. Scale uncertainties are obtained through customary 7-point scale variations with the constraint $1/2 \le \mu_R/\mu_F \le 2$, while correlating the scale variation factors in production and decay. The fiducial cuts are summarized in table 1. If more than two bottom-flavoured jets (b-jets) are present in the final state, the pair with the invariant mass closer to the Higgs-boson mass is chosen.

The fiducial cross sections are $6.261(7)^{+0.9\%}_{-1.8\%}$ fb for MiNNLO$_{PS}$ and $6.348(6)^{+1.2\%}_{-1.4\%}$ fb for NNLOPS. Because of the more exclusive setup, the difference between the MiNNLO$_{PS}$ and NNLOPS predictions is slightly larger than for the inclusive cross section and for W^+H

production in the previous section. Still, the fiducial cross sections agree at the level of 1.4%, which is fully covered by the scale uncertainties. We would like to stress that this level of agreement in the fiducial phase-space volume of the $e^+e^-b\bar{b}$ final state is quite remarkable, given the very small scale dependence of this process.

As far as differential distributions are concerned, in figure 3 we consider the invariant mass of the ZH system (m_{ZH}) and observables related to the bottom quarks from the Higgs decay. In particular, the invariant mass of the b-jet pair (m_{bb}), its transverse momentum ($p_{T,bb}$), and the rapidity difference between the two b-jets ($|\Delta y_{b,b}|$) are shown. We note that the two b here refer to the two b-jets with invariant mass closest to the Higgs mass, as discussed above. Also here we find a good agreement between MiNNLO$_{PS}$ and NNLOPS predictions for all observables within the scale-variation bands, with differences, by and large, lower than 1-2%. Besides statistical fluctuations, these differences are induced by the 1.4% shift in the fiducial cross section noticed before, while the agreement in terms of shapes is even better.

4 Phenomenological results

In this section we present phenomenological results for VH production with $H \to b\bar{b}$ decay in proton-proton collisions at the LHC with a center of mass energy of $\sqrt{s} = 13$ TeV. More precisely, we consider both MiNLO' and MiNNLO$_{PS}$ results for the processes $pp \to e^\pm\nu_e b\bar{b}$ and $pp \to e^+e^-b\bar{b}$, and compare our state-of-the-art MiNNLO$_{PS}$ predictions to recent ATLAS data [131]. Besides integrated inclusive and fiducial cross sections we also discuss differential distributions in the fiducial phase space, and we analyze the effects of using different jet-clustering algorithms.

4.1 Input parameters and settings

We use the NNLO set of the NNPDF31 [148] parton densities with $\alpha_s(m_Z)$=0.118. Our input parameters are set to the following PDG values [149]: $G_F = 1.166379\times10^{-5}$ GeV^{-2}, m_W = 80.379 GeV, $\Gamma_W = 2.085$ GeV, $m_Z = 91.1876$ GeV, $\Gamma_Z = 2.4952$ GeV, $m_H = 125.09$ GeV and $\Gamma_H = 4.1$ MeV. We compute the EW coupling as $\alpha_{EM} = \sqrt{2}G_F m_W^2(1 - m_W^2/m_Z^2)/\pi$ and the mixing angle as $\cos^2\theta_W = m_W^2/m_Z^2$. The $H \to b\bar{b}$ branching ratio is set to Br$_{H\to b\bar{b}}$ = 0.5824. Similarly to what is done in the validation section, in $pp \to HZ \to e^+e^-b\bar{b}$ we include contributions in which the Higgs boson is radiated from a heavy quark loop, setting the pole mass of the bottom quark to $m_b = 4.78$ GeV and the pole mass of the top quark to $m_t = 172.5$ GeV. The bottom Yukawa coupling is set to $y_b(m_H) = 1.280 \times10^{-2}$, which, however, as pointed out in section 2.4, cancels out in the ration of eq. (2.5) when combining production and decay events. We employ Pythia8 [132] with the Monash tune [150] for all matched predictions. We do not include any effect from hadronization, underlying event modelling or a QED shower, except for the comparison to data in section 4.5.

Besides a fully inclusive setup, which we refer to as `inclusive`, we consider two sets of fiducial cuts. The first one is inspired by the CERN Yellow Report [146] and is refereed to as `fiducial-YR`. The second set of cuts is taken from ref. [131] and is referred to as `fiducial-ATLAS`. Both sets of fiducial cuts are summarized in table 2.

fiducial-YR [146]	
$pp \to W^{\pm}H \to e^{\pm}\nu_e b\bar{b}$	$pp \to ZH \to e^+e^- b\bar{b}$
$p_{\mathrm{T},e} > 15\,\mathrm{GeV}$, $p_{\mathrm{T,miss}} > 15\,\mathrm{GeV}$, $|\eta_e| < 2.5$	$p_{\mathrm{T},e} > 15\,\mathrm{GeV}$, $|\eta_e| < 2.5$
	$75\,\mathrm{GeV} < m_{e^+e^-} < 105\,\mathrm{GeV}$
≥ 2 b-jets (anti-k_T [151], R=0.4)	≥ 2 b-jets (anti-k_T [151], R=0.4)
$p_{\mathrm{T},b\text{-jet}} > 25\,\mathrm{GeV}$, $|\eta_{b\text{-jet}}| < 2.5$	$p_{\mathrm{T},b\text{-jet}} > 25\,\mathrm{GeV}$, $|\eta_{b\text{-jet}}| < 2.5$
fiducial-ATLAS [131]	
$pp \to W^{\pm}H \to \ell^{\pm}\nu_{\ell} b\bar{b}$	$pp \to ZH \to \ell^+\ell^- b\bar{b}/\nu_{\ell}\bar{\nu}_{\ell} b\bar{b}$
$|y_H| < 2.5$	$|y_H| < 2.5$
categories:	categories:
$p_{\mathrm{T},W} \in [250,400]\,\mathrm{GeV}$,	$p_{\mathrm{T},Z} \in [250,400]\,\mathrm{GeV}$,
$p_{\mathrm{T},W} \in [400, \infty]\,\mathrm{GeV}$	$p_{\mathrm{T},Z} \in [400, \infty]\,\mathrm{GeV}$

Table 2. Fiducial cuts used in the setup `fiducial-YR` and setup `fiducial-ATLAS`.

4.2 Inclusive and fiducial cross sections

We start by discussing integrated cross section both in the fully inclusive case and including fiducial cuts. In table 3 we report MiNLO′ and MiNNLO$_{\mathrm{PS}}$ prediction for both the neutral and the charged-current VH production processes with $H \to b\bar{b}$ decay. For ZH production we report separately the numbers with and without the gluon-fusion contribution that is induced by a closed heavy-quark loop (top and bottom). The inclusive cross sections are in good agreement with the NNLO predictions from VH@NNLO refs. [44–46, 152] that are obtained in the on-shell approximation with $\mu_{\mathrm{R}} = \mu_{\mathrm{F}} = m_{VH}$. Assuming branching ratios consistent with our calculation ($\mathrm{Br}_{H \to b\bar{b}} = 0.5824$, $\mathrm{Br}_{W^{\pm} \to e^{\pm}\nu_e} = 0.10898$ and $\mathrm{Br}_{Z \to e^+e^-} = 0.033628$), they read $\sigma_{W^+H \to e^+\nu_e b\bar{b}} = 58.3^{+0.2\%}_{-0.3\%}$ fb, $\sigma_{W^-H \to e^-\nu_e b\bar{b}} = 36.3^{+0.2\%}_{-0.3\%}$ fb, $\sigma^{\mathrm{no}\ gg \to ZH}_{ZH \to e^+e^- b\bar{b}} = 16.0^{+0.2\%}_{-0.3\%}$ fb, and $\sigma^{\mathrm{with}\ gg \to ZH}_{ZH \to e^+e^- b\bar{b}} = 17.0^{+1.5\%}_{-1.2\%}$ fb.[1] We note that the inclusive on-shell calculation differs from the MiNNLO$_{\mathrm{PS}}$ also with respect to the scale settings and the different treatment of terms beyond accuracy.

Furthermore, we find in table 3 that MiNNLO$_{\mathrm{PS}}$ induces a correction of about 5–6% with respect to MiNLO′, both in the fully inclusive and in the fiducial phase space volume, disregarding the loop-induced gg contribution in the case of ZH production. While for the inclusive cross sections MiNLO′ and MiNNLO$_{\mathrm{PS}}$ predictions are compatible within scale variations, the MiNNLO$_{\mathrm{PS}}$ corrections in the fiducial phase space are generally not covered by plain scale variations when correlating the scales in production and decay. If

---

[1]As far as the terms mediated by a closed top-quark loop are concerned, the cross sections computed with VH@NNLO have been obtained switching off both the R_{I} and V_{I} terms for the $W^{\pm}H$ case, whereas for the ZH case we kept the $R_{\mathrm{I/II}}$ contributions, just like in our calculation.

$pp \rightarrow W^+H \rightarrow e^+\nu_e b\bar{b}$		
σ [fb]	inclusive	fiducial-YR
MiNLO$'$	$54.04^{+6.6\%}_{-3.6\%}$	$20.13^{+2.3\%}_{-3.1\%}$
MiNNLO$_{\text{PS}}$	$57.44^{+1.7\%}_{-0.8\%}$	$21.27^{+1.3\%}_{-1.3\%}$

$pp \rightarrow W^-H \rightarrow e^-\bar{\nu}_e b\bar{b}$		
σ [fb]	inclusive	fiducial-YR
MiNLO$'$	$33.82^{+6.6\%}_{-3.6\%}$	$13.07^{+2.4\%}_{-3.3\%}$
MiNNLO$_{\text{PS}}$	$35.87^{+1.5\%}_{-0.7\%}$	$13.77^{+1.5\%}_{-1.6\%}$

$pp \rightarrow ZH \rightarrow e^+e^- b\bar{b}$		
σ [fb]	inclusive	fiducial-YR
MiNLO$'$	$14.88^{+6.7\%}_{-3.7\%}$	$5.21^{+2.2\%}_{-3.0\%}$
MiNNLO$_{\text{PS}}$ (no $gg \rightarrow ZH$)	$15.79^{+1.8\%}_{-0.9\%}$	$5.48^{+1.2\%}_{-1.2\%}$
MiNNLO$_{\text{PS}}$ (with $gg \rightarrow ZH$)	$16.99^{+3.6\%}_{-2.3\%}$	$6.07^{+3.4\%}_{-2.9\%}$

Table 3. Integrated cross sections for the $e^+\nu_e b\bar{b}$, $e^-\bar{\nu}_e b\bar{b}$ and $e^+e^- b\bar{b}$ final states in the `inclusive` and the `fiducial-YR` setup.

we vary the scales in production and decay in an uncorrelated manner, the unnaturally small MiNLO$'$ uncertainty band in the fiducial setup increases and the predictions become compatible within scale variations. The scale uncertainties of MiNNLO$_{\text{PS}}$ are significantly smaller than the ones of MiNLO$'$ in either case, with a reduction by more than a factor of two. Considering the loop-induced $gg \rightarrow ZH$ contribution, its effect is quite significant. It contributes about almost 8% in the inclusive and almost 11% in the fiducial phase space to the MiNNLO$_{\text{PS}}$ cross sections. As pointed out before, the contribution from loop-induced gg diagrams dominates the current theoretical uncertainties. Thus, including NLO QCD corrections to the $gg \rightarrow ZH$ process in the matching to parton showers is a crucial next step.[2]

4.3 Distributions in the fiducial phase space

We continue our presentation of phenomenological results by considering differential distributions in the `fiducial-YR` phase space defined in table 2. Figures 4 and 5 show various observables for $e^+\nu_e b\bar{b}$ (W^+H) and $e^+e^- b\bar{b}$ (ZH) production, respectively.[3]

In particular, the invariant mass (m_{bb}) and transverse momentum ($p_{\text{T},bb}$) of the bottom-quark pair, the absolute rapidity difference between the two bottom quarks ($|\Delta y_{b,b}|$), the

---

[2]Recently, substantial progress was made in the calculation of the relevant two-loop amplitude to (on-shell) $gg \rightarrow ZH$ production [54–56] and a first calculation at NLO QCD in a small mass expansion was achieved [53].

[3]The corresponding results for $e^-\nu_e b\bar{b}$ (W^-H) production are shown in appendix A.
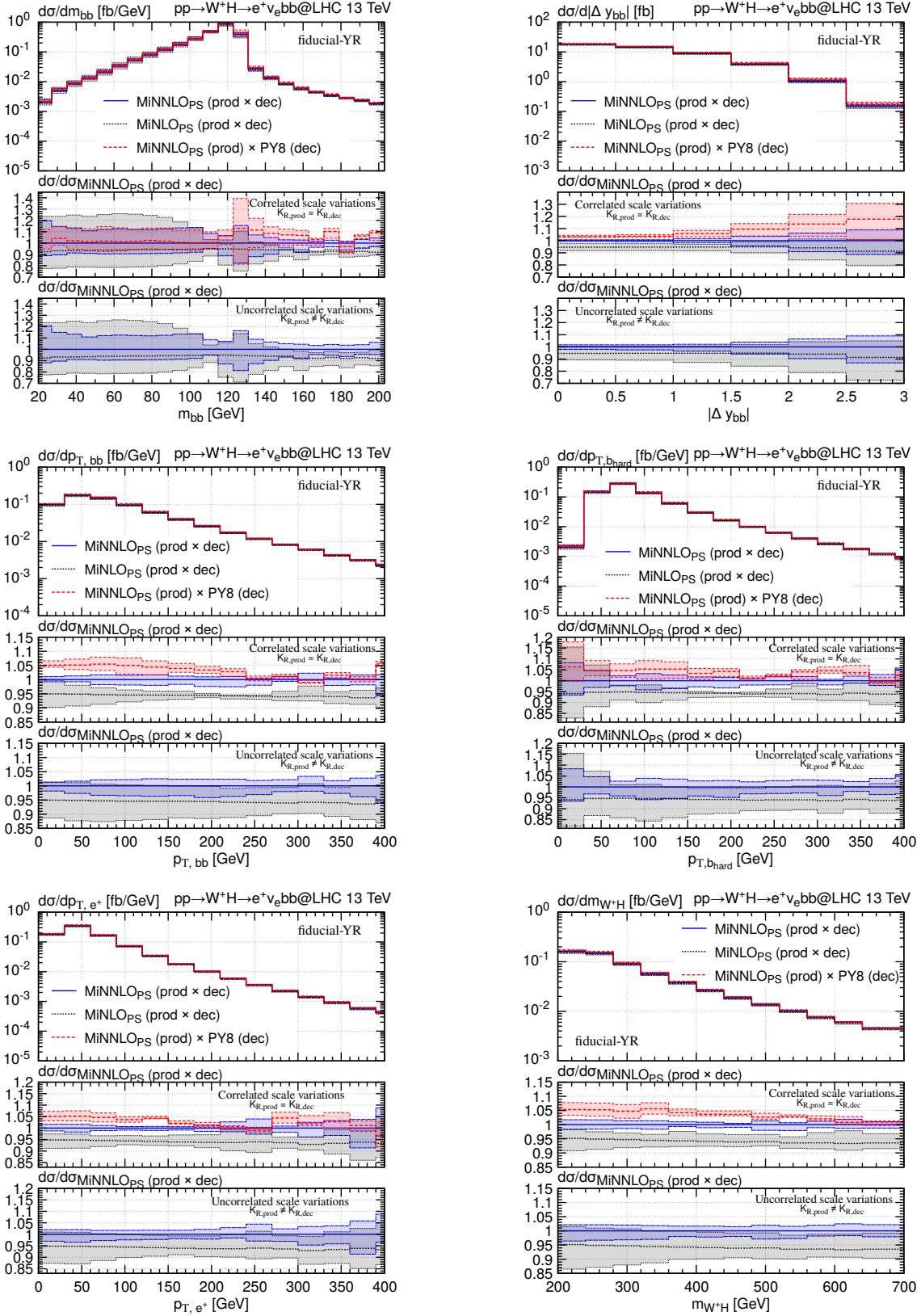
Figure 4. Differential distributions for $e^+\nu_e b\bar{b}$ production with `fiducial-YR` cuts. $K_{\mathrm{R,prod}}$ and $K_{\mathrm{R,dec}}$ refer to the variation factors of the renormalization scales of production and decay, respectively.
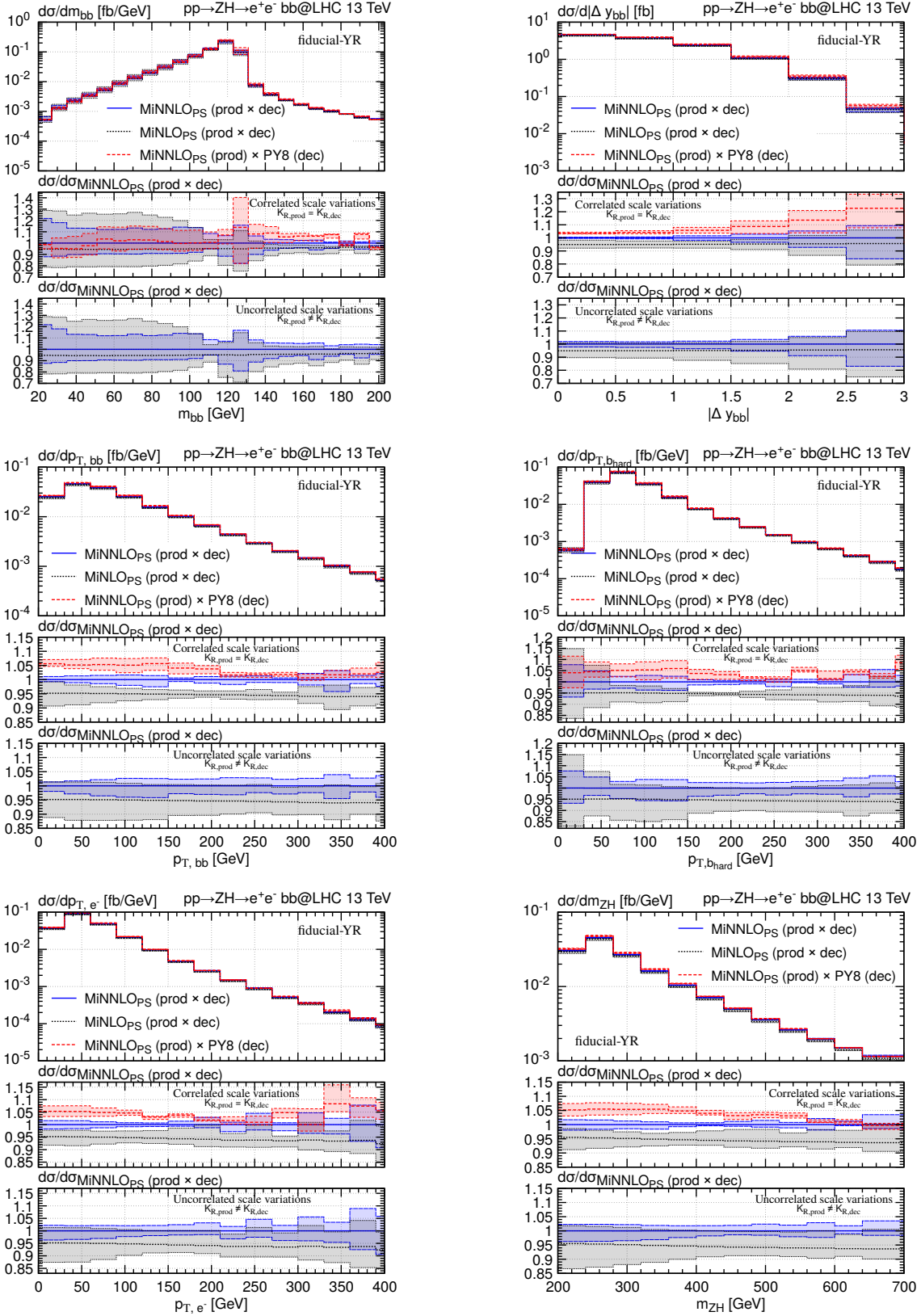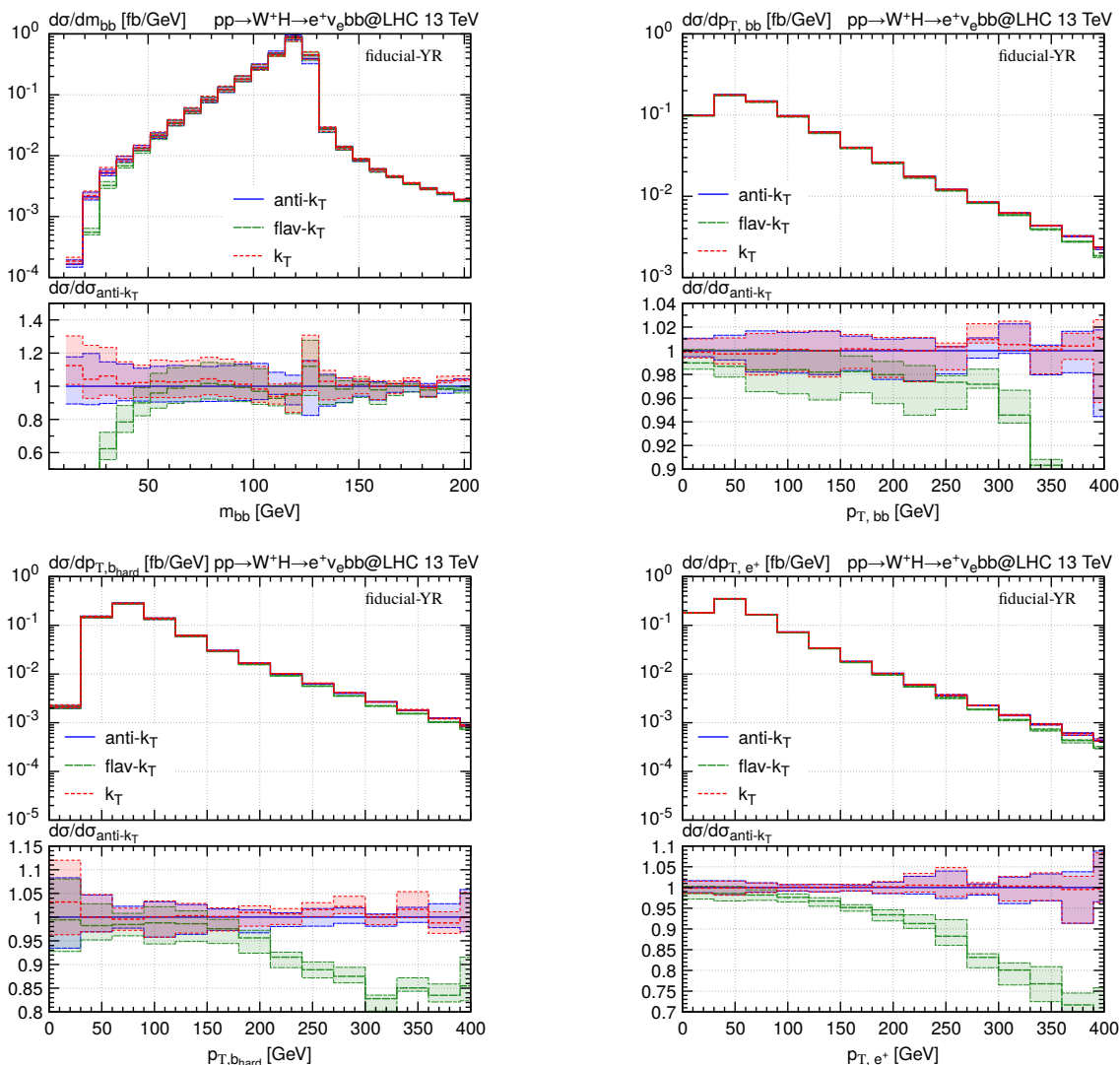
Figure 5. Differential distributions for $e^+e^-b\bar{b}$ production with `fiducial-YR` cuts. $K_{\mathrm{R,prod}}$ and $K_{\mathrm{R,dec}}$ refer to the variation factors of the renormalization scales of production and decay, respectively.

transverse momentum of the hardest bottom quark ($p_{\mathrm{T},b_{\mathrm{hard}}}$), the transverse momentum of the positron/electron ($p_{\mathrm{T},e^+}/p_{\mathrm{T},e^-}$), and the invariant mass of the colour-singlet system in the final state (m_{WH}/m_{ZH}) are shown. We recall that with the two bottom quarks (from the Higgs decay) we actually denote the two jets with at least one bottom quark whose invariant mass is closest to the Higgs-boson mass. The plots are organized as follows: the main frame includes the full MiNNLO$_{\mathrm{PS}}$ prediction (blue, solid), the full MiNLO$'$ prediction (black, dotted), and the MiNNLO$_{\mathrm{PS}}$ prediction with LO decay through Pythia8 (red, dashed) as absolute cross sections of the differential distributions. The lower two insets show the ratio to the MiNNLO$_{\mathrm{PS}}$ central prediction, where in the first inset scale uncertainties are evaluated by assuming that the 7-point scale dependence in production and decay is fully correlated, while in the second inset uncorrelated scale variations in production and decay are performed, but excluding the extreme variations (one scale up, the other down). When the Higgs decay is simulated by Pythia8, the scale variation is also handled by Pythia8 using its so-called "automated parton-shower variation" facility [153]. In particular, we vary the renormalisation scale for final-state radiation by a factor 2 around the central value, correlating this variation with the one performed in the production stage. The relative behaviour observed in both the $W^\pm H$ and the ZH results is very similar. Thus, we can discuss the sets of plots simultaneously.

Looking at the m_{bb} distribution, we notice that MiNLO$'$ and MiNNLO$_{\mathrm{PS}}$ predictions are very similar as far as the shape is concerned, while the MiNNLO$_{\mathrm{PS}}$ corrections increase the cross section by roughly 5%, as already observed for the integrated fiducial cross section in the previous section. MiNLO$'$ and MiNNLO$_{\mathrm{PS}}$ predictions are fully compatible within scale variations, regardless of whether scale variations are assumed to be correlated or uncorrelated. Interestingly, for this observable the two cases lead to very similar uncertainties, which can be seen by comparing the first and the second ratio inset. Moreover, we observe clearly reduced scale uncertainties for MiNNLO$_{\mathrm{PS}}$ compared to MiNLO$'$ below the Higgs-mass threshold by roughly a factor of two, but similarly large uncertainties above the threshold. Using Pythia8 to include the $H \to b\bar{b}$ decay at LO compares rather well to using the full MiNNLO$_{\mathrm{PS}}$ prediction for production and decay.

For the rapidity difference of the two bottom quarks MiNLO$'$ and MiNNLO$_{\mathrm{PS}}$ predictions are not compatible at central rapidities when assuming correlated uncertainties. In particular, the MiNNLO$_{\mathrm{PS}}$ result features a very small band at the $\pm 1\%$ level. By uncorrelating the scale variation in production and decay more realistic scale bands are obtained, leading to fully compatible MiNLO$'$ and MiNNLO$_{\mathrm{PS}}$ predictions, where the uncertainties of the latter increase only to a very few percent. This behaviour can be observed also for the remaining distributions, where it is visible almost over the entire plotted ranges. This justifies a more conservative uncertainty estimate by taking uncorrelated scale variations in production and decay. We also observe that the LO $H \to b\bar{b}$ decay through Pythia8 is insufficient to describe this observable accurately, especially in the forward $\Delta y_{b,b}$ region. Moreover, in the central rapidity region, the uncertainty bands of the Pythia8-decayed results are not compatible with the MiNNLO$_{\mathrm{PS}}$ ones.

Considering the other differential observables it is clear that similar features appear. For all of them MiNNLO$_{\mathrm{PS}}$ induces a mostly flat $\sim 5\%$ correction on top of MiNLO$'$

Figure 6. Differential distributions for $e^+\nu_e b\bar{b}$ production with `fiducial-YR` cuts using different jet-clustering algorithms, all with $R = 0.4$.

and leads to a significant reduction of the scale uncertainties. Note that for correlated scale uncertainties some accidental cancellations in the scale variations occur, which are particularly visible from the MiNLO′ scale-uncertainty band around $200\,\mathrm{GeV}$ in both the $p_{T,bb}$ and $p_{T,b_{\mathrm{hard}}}$ distributions. The red curve that includes the $H \to b\bar{b}$ decay through PYTHIA8 at LO is in shape rather similar to the full MiNNLO$_{\mathrm{PS}}$ result, but it is roughly 5% above the full MiNNLO$_{\mathrm{PS}}$ prediction and thereby outside the quoted scale uncertainties in various phase-space regions.

4.4 Impact of jet-clustering algorithms

In this section we address the impact of different jet-clustering algorithms in the definition of b-jets on differential distributions. Our calculations are based on matrix elements with massless bottom quarks in the final state. Therefore, performing an event simulation is particularly important as it allows us to include a finite bottom-quark mass in the generation

– 20 –

of Les Houches events or through Pythia when showering the events. This makes it possible to perform any standard jet clustering to define b-jets, which in a massless calculation would otherwise lead to infrared (IR) unsafe results. For massless b-jets, for instance in a fixed-order calculation, it is instead possible to use the flavour-k_T algorithm of ref. [147] for an IR-safe definition of b-jets.

Figure 6 shows the m_{bb}, $p_{T,bb}$, $p_{T,b_{\text{hard}}}$, and p_{T,e^+} distributions for W^+H production in the `fiducial-YR` phase-space defined in table 2. The different curves correspond to using the anti-k_T [151] (blue, solid), the flavour-k_T [147] (green, long-dashed), and the k_T [154] (red, short-dashed) jet-clustering algorithm, all with $R = 0.4$. In the bottom panels we show the ratio to the anti-k_T result. It is easy to see that the anti-k_T and k_T algorithms lead to very compatible results with small differences only in certain phase-space regimes, in particular for the m_{bb} distribution. There is a 5–10% difference between anti-k_T and k_T clustering both at small m_{bb} and at the m_H threshold. Such differences are not unexpected and they originate from soft gluons being more likely to be clustered in the b-jets with the k_T algorithm.

As far as the flavour-k_T algorithm is concerned, the differences to the other two approaches are much more prominent in some regions of phase-space. The flavour-k_T algorithm assumes b-jets to originate only from jets that contain an uneven number of bottom quarks, since an even number of bottom quarks in one jet typically originates from $g \to b\bar{b}$ splittings, which in the flavour-k_T algorithm shall not be considered as b-jets. The reason for adopting such treatment stems mostly from fixed-order calculations in the massless approximation of bottom quarks, i.e. in the five-flavour scheme (5FS), where the standard clustering algorithms lead to definitions of bottom-quark jets that are not IR safe, as discussed before. Clear differences of the flavour-k_T results to the non-flavour specific clustering algorithms are observed at small m_{bb} and at large values of $p_{T,bb}$, $p_{T,b_{\text{hard}}}$, and p_{T,e^+}. Additionally, around the $m_{bb} \sim m_H$ threshold the flavour-k_T curve follows the one of the standard k_T algorithm and shows a similar difference to the anti-k_T one, as both the flavour and the standard k_T algorithm use the same measure in the ordering of the jet clustering. In order to explain these differences we focus on a comparison between k_T and flavour-k_T algorithms since the underlying distance measure is more closely related.

We remind the reader how the flavour-k_T algorithm works. The clustering procedure is the same as any sequential algorithm but the distance measure is modified as follows:

$$d_{ij}^{(F)} = \frac{\left(\Delta\eta_{ij}^2 + \Delta\phi_{ij}^2\right)}{R^2} \times \begin{cases} \max\left(p_{T,i}^2, p_{T,j}^2\right), & \text{softer of } i, j \text{ is flavoured,} \\ \min\left(p_{T,i}^2, p_{T,j}^2\right), & \text{softer of } i, j \text{ is flavourless,} \end{cases} \quad (4.1)$$

where *softer* means with lower p_T. The distance with the beam is defined separating explicitly the beam moving towards positive rapidities B (right-moving beam) and the opposite beam towards negative rapidities $\bar{B}$ (left-moving beam),

$$d_{iB}^{(F)} = \begin{cases} \max\left(p_{T,i}^2, p_{T,B}^2\right), & i \text{ is flavoured,} \\ \min\left(p_{T,i}^2, p_{T,B}^2\right), & i \text{ is flavourless,} \end{cases} \quad (4.2)$$

$$d_{i\bar{B}}^{(F)} = \begin{cases} \max\left(p_{T,i}^2, p_{T,\bar{B}}^2\right), & i \text{ is flavoured,} \\ \min\left(p_{T,i}^2, p_{T,\bar{B}}^2\right), & i \text{ is flavourless,} \end{cases} \quad (4.3)$$

where $p_{\mathrm{T},B}$ ($p_{\mathrm{T},\bar{B}}$) represents the hard transverse scale associated with the right-moving (left-moving) beam, defined as follows:

$$p_{\mathrm{T},B}(\eta) = \sum_i p_{\mathrm{T},i} \left(\Theta(\eta_i - \eta) + \Theta(\eta - \eta_i) e^{\eta_i - \eta} \right) , \qquad (4.4)$$

$$p_{\mathrm{T},\bar{B}}(\eta) = \sum_i p_{\mathrm{T},i} \left(\Theta(\eta - \eta_i) + \Theta(\eta_i - \eta) e^{\eta - \eta_i} \right) . \qquad (4.5)$$

If the smallest distance is a d_{ij}, then the two (pseudo) particles are clustered together into a (pseudo) particle whose flavour is given by the sum of the two individual flavours. In particular, when a bottom-flavoured particle and anti-particle end up in the same jet, they will give rise to a non-flavoured jet. If the smallest distance is a d_{ib}, the (pseudo) particle is considered as a final jet and removed from the clustering sequence.

The large discrepancy between flavour-k_T and k_T results at small m_{bb}, which is dominated by small ΔR_{bb} values, is due to a different treatment of particular kinematic regions in the two algorithms. Specifically, when two b-quarks are separated by $\Delta R_{bb} > R$, the k_T algorithm typically reconstructs two b-jets. On the other hand, the flavour-k_T algorithm compares the relative distance d_{ij} with the distance of each bottom quark to the beam $d_{bB}^{(F)}$ ($d_{b\bar{B}}^{(F)}$). The latter quantity is by constuction larger than the individual transverse momenta of the bottom and anti-bottom quarks. Since d_{ij} can be smaller than $d_{bB}^{(F)}$ ($d_{b\bar{B}}^{(F)}$) even for $\Delta R_{bb} > R$, the two bottom quarks can be clustered even if $\Delta R_{bb} > R$. Similar arguments apply also in the region of large transverse momenta, since when the Higgs boson is highly boosted, its decay products tend to be collimated.

Apart from that, we note that even for bottom quarks with $\Delta R_{bb} < R$ the output of the two clustering algorithms can be different: in this case, both algorithms tend to cluster the two bottom quarks together, giving rise to a b-jet in the k_T algortihm and a gluon-jet in the flavour-k_T one. It is thus more likely that the event passes the fiducial cuts in the k_T case, because of the presence of one additional secondary bottom quark. In this context a soft b is often sufficient as it can be promoted to a hard b-jet by clustering with a hard gluon. This clustering mechanism is instead strongly suppressed in the flavour-k_T one. In this case the anti-k_T and k_T algorithms do not actually reconstruct the two hard b-jets originating from the Higgs-boson decay.

Overall, it is clear that in various phase-space regions the flavour-k_T clustering leads to significant changes. It is therefore not advisable to use this approach for theoretical predictions, unless the same clustering is used also on the experimental side, which is usually not the case. In fact, the application of the flavour-k_T algorithm to experimental data is challenging, as discussed in ref. [155]. Alternatively, one should include a theoretical estimate of the size of the discrepancy due to the use of different algorithms in the theory simulations and measurements. While in fixed-order calculations in the 5FS such approach is mandatory to obtain IR-safe results as far as bottom-quark tagging is concerned, in exclusive event simulations matched to parton showers this problem can be circumvented by including the bottom-quark mass through reshuffling the final-state momenta of the bottom quarks, so that flavour-k_T clustering can be avoided. This is an example why matching high accuracy calculations at fixed order and parton showers is important and
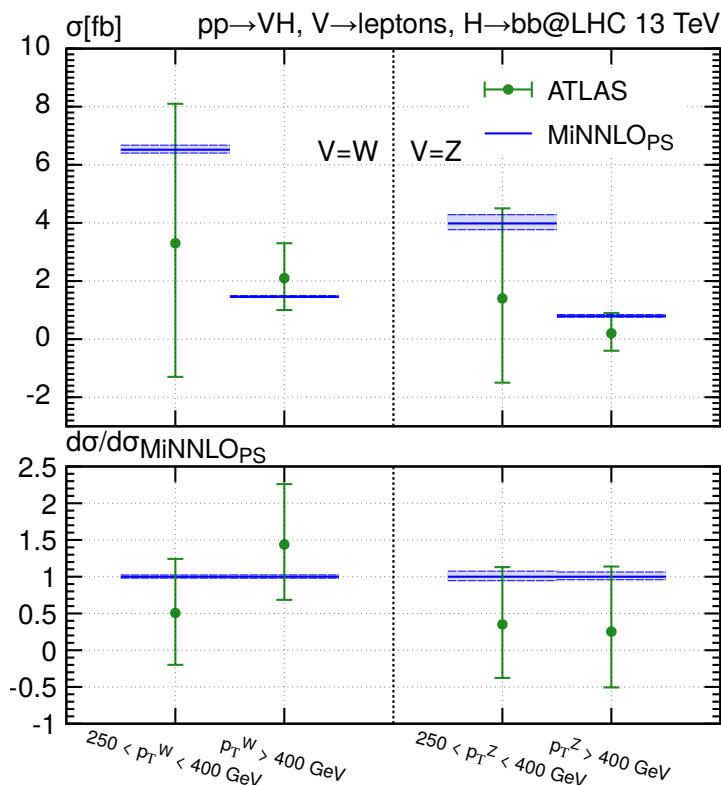
Figure 7. Comparison of MiNNLO$_{\text{PS}}$ predictions to ATLAS data [131].

advantageous. One should bear in mind, however, that such reshuffling is not completely unambiguous and comes with some uncertainties on the bottom-quark kinematics. Thus, ideally the bottom-quark kinematics should be described using massive bottom quarks at amplitude level, i.e. a four-flavour scheme (4FS) calculation, but this is not always feasible at high accuracy with current technology and also comes with other shortcomings [156]. Furthermore, it is important to be aware that in certain configurations a hard reconstructed *b*-jet can come from a soft bottom quark and that the two selected *b*-jets may actually not originate from the Higgs-boson decay. These occurrences are less likely when using the flavour-k_T algorithm.

4.5 Comparison to ATLAS data

Figure 7 compares our MiNNLO$_{\text{PS}}$ predictions to recent ATLAS data [131]. The respective cross sections are reported in table 4. The results correspond to $W^{\pm}H$ and ZH production with all leptonic final states, i.e. $\ell^{\pm}\nu_{\ell}b\bar{b}$, $\ell^{+}\ell^{-}b\bar{b}$ and $\nu_{\ell}\bar{\nu}_{\ell}b\bar{b}$ with $\ell \in \{e, \mu, \tau\}$. For this comparison we have included hadronization effects through PYTHIA8, which however have a negligible impact. It is clear that the measured VH cross sections are fully compatible with our predictions within uncertainties. However, one must bear in mind that this measurement requires relatively large lower cuts on the transverse momentum of the vector boson. Therefore, the experimental error is quite large, being dominated mostly by the limited statistics. In fact, within the current experimental uncertainties the measured cross

$pp \to W^{\pm}H \to \ell^{\pm}\nu_\ell b\bar{b}$		
σ [fb]	$p_T^W \in [250,400]\,\mathrm{GeV}$	$p_T^W \in [400,\,\infty]\,\mathrm{GeV}$
MiNNLO$_{\mathrm{PS}}$	$6.52^{+2.4\%}_{-1.8\%}$	$1.46^{+2.5\%}_{-1.9\%}$
ATLAS [131]	$3.3^{+3.6(\mathrm{Stat.})+3.2(\mathrm{Syst.})}_{-3.4(\mathrm{Stat.})-3.0(\mathrm{Syst.})}$	$2.1^{+1.0(\mathrm{Stat.})+0.6(\mathrm{Syst.})}_{-0.9(\mathrm{Stat.})-0.5(\mathrm{Syst.})}$
$pp \to ZH \to (\ell^+\ell^-,\nu_\ell\bar{\nu}_\ell)b\bar{b}$		
σ [fb]	$p_T^Z \in [250,400]\,\mathrm{GeV}$	$p_T^Z \in [400,\,\infty]\,\mathrm{GeV}$
MiNNLO$_{\mathrm{PS}}$	$3.98^{+7.6\%}_{-5.4\%}$	$0.79^{+6.5\%}_{-4.2\%}$
ATLAS [131]	$1.4^{+2.4(\mathrm{Stat.})+1.9(\mathrm{Syst.})}_{-2.3(\mathrm{Stat.})-1.7(\mathrm{Syst.})}$	$0.2^{+0.6(\mathrm{Stat.})+0.3(\mathrm{Syst.})}_{-0.5(\mathrm{Stat.})-0.3(\mathrm{Syst.})}$

Table 4. Fiducial cross sections in the `fiducial-ATLAS` setup compared to data.

sections are compatible with zero within one standard deviation. It will be interesting to see how this comparison will develop when the experiments have collected more data. Moreover, the original publications [3, 4], where the $H \to b\bar{b}$ decay was observed, involved a cut of only 150 GeV on the transverse momentum of the vector boson, but no unfolding to fiducial cross sections was performed. Therefore, repeating the exclusive data–theory comparison at the fiducial level including a cut of only 150 GeV on vector-boson transverse momentum would be desirable in the future.

5 Conclusions

We have presented novel predictions for VH production with $H \to b\bar{b}$ decay within the MiNNLO$_{\mathrm{PS}}$ framework. NNLO QCD accuracy is retained for both production and decay, while the matching to the Pythia8 parton shower ensures a fully realistic exclusive description of the process at the level of hadronic events. For the $W^{\pm}H$ process NNLO+PS accuracy is achieved for the first time for production and decay.

Our results have been validated against earlier calculations using the NNLOPS approach, which exploits a numerically intensive multidifferential reweighting to upgrade MiNLO$'$ events to NNLO QCD accuracy a posteriori. We find fully compatible results within scale uncertainties when comparing our MiNNLO$_{\mathrm{PS}}$ predictions to earlier NNLOPS results for $W^{\pm}H$ production with an on-shell Higgs boson and for ZH production including the $H \to b\bar{b}$ at NNLO+PS. The agreement is particularly remarkable considering the fact that the scale uncertainties of both predictions are at the level of only 1–2% in most phase-space regions. Given that the reweighting procedure of the NNLOPS approach induces some (technical) limitations and for VH production it relies on certain approximations in describing the vector-boson decay, our new MiNNLO$_{\mathrm{PS}}$ VH generator, which includes NNLO corrections on-the-fly directly during the usual Powheg event generation, lifts those shortcomings and can be considered to supersede the previous NNLOPS implementation. We stress, however, that the NNLOPS predictions can still be useful to assess residual uncertainties.

Phenomenological results have been discussed in detail for both the $pp \to e^{\pm}\nu_e b\bar{b}$ and $pp \to e^+ e^- b\bar{b}$ processes at the level of inclusive and fiducial cross section as well as for differential distributions in the fiducial phase space. We find that the NNLO corrections induced by the MiNNLO$_{\mathrm{PS}}$ procedure with respect to MiNLO′ increase both the inclusive and fiducial cross sections by roughly $5-6\%$, while the corrections are relatively flat in phase space for the observables under consideration. Moreover, due to the relatively small scale dependence of the VH processes, uncorrelating scale variations in production and decay to estimate the perturbative uncertainties is crucial to obtain MiNLO′ and MiNNLO$_{\mathrm{PS}}$ results that are compatible within their scale bands. Regardless of this, we observe a clear reduction of scale uncertainties, by roughly a factor of two, when including the MiNNLO$_{\mathrm{PS}}$ corrections. As far as the $H \to b\bar{b}$ decay is concerned, we have shown that including the full NNLO QCD corrections induces important effects with respect to a LO description through Pythia8 for various observables: for the cuts under consideration, they shift the fiducial cross section by about -5% and induce relevant shape effects. In some cases, these effects are not captured by the scale-variation uncertainty from Pythia8. Finally, our results are in agreement with current ATLAS data, keeping in mind that with the current experimental accuracy the measured VH cross section is still compatible with zero.

While at the level of the matrix elements our calculations involve massless bottom quarks, kinematic bottom-mass effects are included approximately through a reshuffling of the bottom quarks at LHE level. In this setup, we have compared the anti-k_T, k_T and flavour-k_T algorithms. The anti-k_T and k_T algorithms give rather similar results, and in the bulk region of the phase space this is also the case for the flavour-k_T algorthim. However, in some phase-space regions, such as at small m_{bb} and at large transverse momenta, we observe substantial differences in the flavour-k_T case. Since experimental analyses usually employ the standard (anti-)k_T algorithm, it is important to be aware of these differences and features, especially when using different jet-clustering algorithms in the theoretical calculations and in experimental measurements.

We have performed largely independent implementations in both Powheg-Box-V2 and Powheg-Box-Res, whose results are fully consistent. We reckon that our MiNNLO$_{\mathrm{PS}}$ VH generators will be very useful for future analyses of these processes in Run III and, in particular, for the High Luminosity LHC phase. Therefore, we will make all relevant codes to simulate NNLO+PS events for the $e^{\pm}\nu_e b\bar{b}$ and $e^+ e^- b\bar{b}$ final states publicly available within the Powheg-Box-Res framework.
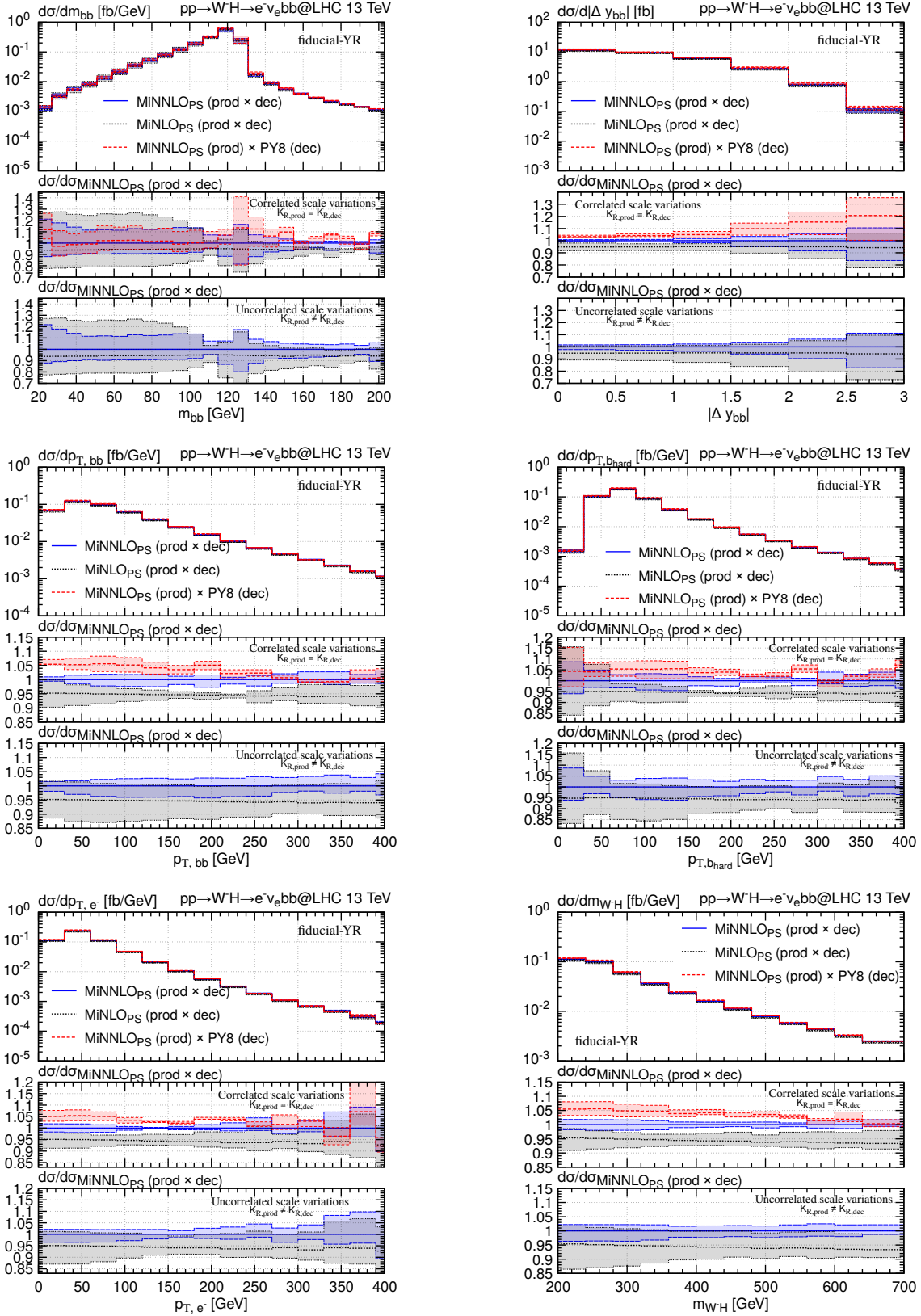
Acknowledgments

A Results for W^-H production

In this section, we report results for W^-H productions. Figure 8 shows plots corresponding to those presented for W^+H production in section 4.3. Since the same conclusions that were drawn for W^+H production in that section hold also for the W^-H process we refrain from commenting on the results further.

Figure 8. Differential distributions for $e^- \bar{\nu} b \bar{b}$ production with `fiducial-YR` cuts. $K_{\mathrm{R,prod}}$ and $K_{\mathrm{R,dec}}$ refer to the variation factors of the renormalization scales of production and decay, respectively.

References

[1] ATLAS collaboration, *Observation of a new particle in the search for the Standard Model Higgs boson with the ATLAS detector at the LHC*, *Phys. Lett. B* **716** (2012) 1 [`arXiv:1207.7214`] [ɪɴSPIRE].

[2] CMS collaboration, *Observation of a New Boson at a Mass of* 125 *GeV with the CMS Experiment at the LHC*, *Phys. Lett. B* **716** (2012) 30 [`arXiv:1207.7235`] [ɪɴSPIRE].

[3] ATLAS collaboration, *Observation of* $H \to b\bar{b}$ *decays and* VH *production with the ATLAS detector*, *Phys. Lett. B* **786** (2018) 59 [`arXiv:1808.08238`] [ɪɴSPIRE].

[4] CMS collaboration, *Observation of Higgs boson decay to bottom quarks*, *Phys. Rev. Lett.* **121** (2018) 121801 [`arXiv:1808.08242`] [ɪɴSPIRE].

[5] J.M. Butterworth, A.R. Davison, M. Rubin and G.P. Salam, *Jet substructure as a new Higgs search channel at the LHC*, *Phys. Rev. Lett.* **100** (2008) 242001 [`arXiv:0802.2470`] [ɪɴSPIRE].

[6] G. Ferrera, M. Grazzini and F. Tramontano, *Associated WH production at hadron colliders: a fully exclusive QCD calculation at NNLO*, *Phys. Rev. Lett.* **107** (2011) 152003 [`arXiv:1107.1164`] [ɪɴSPIRE].

[7] G. Ferrera, M. Grazzini and F. Tramontano, *Associated ZH production at hadron colliders: the fully differential NNLO QCD calculation*, *Phys. Lett. B* **740** (2015) 51 [`arXiv:1407.4747`] [ɪɴSPIRE].

[8] G. Ferrera, G. Somogyi and F. Tramontano, *Associated production of a Higgs boson decaying into bottom quarks at the LHC in full NNLO QCD*, *Phys. Lett. B* **780** (2018) 346 [`arXiv:1705.10304`] [ɪɴSPIRE].

[9] J.M. Campbell, R.K. Ellis and C. Williams, *Associated production of a Higgs boson at NNLO*, *JHEP* **06** (2016) 179 [`arXiv:1601.00658`] [ɪɴSPIRE].

[10] R.V. Harlander and W.B. Kilgore, *Higgs boson production in bottom quark fusion at next-to-next-to leading order*, *Phys. Rev. D* **68** (2003) 013001 [`hep-ph/0304035`] [ɪɴSPIRE].

[11] R.V. Harlander, K.J. Ozeren and M. Wiesemann, *Higgs plus jet production in bottom quark annihilation at next-to-leading order*, *Phys. Lett. B* **693** (2010) 269 [`arXiv:1007.5411`] [ɪɴSPIRE].

[12] R. Harlander and M. Wiesemann, *Jet-veto in bottom-quark induced Higgs production at next-to-next-to-leading order*, *JHEP* **04** (2012) 066 [`arXiv:1111.2182`] [ɪɴSPIRE].

[13] S. Bühler, F. Herzog, A. Lazopoulos and R. Müller, *The fully differential hadronic production of a Higgs boson via bottom quark fusion at NNLO*, *JHEP* **07** (2012) 115 [`arXiv:1204.4415`] [ɪɴSPIRE].

[14] S. Marzani, R.D. Ball, V. Del Duca, S. Forte and A. Vicini, *Higgs production via gluon-gluon fusion with finite top mass beyond next-to-leading order*, *Nucl. Phys. B* **800** (2008) 127 [`arXiv:0801.2544`] [ɪɴSPIRE].

[15] R.V. Harlander and K.J. Ozeren, *Finite top mass effects for hadronic Higgs production at next-to-next-to-leading order*, *JHEP* **11** (2009) 088 [arXiv:0909.3420] [INSPIRE].

[16] R.V. Harlander, H. Mantler, S. Marzani and K.J. Ozeren, *Higgs production in gluon fusion at next-to-next-to-leading order QCD for finite top mass*, *Eur. Phys. J. C* **66** (2010) 359 [arXiv:0912.2104] [INSPIRE].

[17] A. Pak, M. Rogal and M. Steinhauser, *Finite top quark mass effects in NNLO Higgs boson production at LHC*, *JHEP* **02** (2010) 025 [arXiv:0911.4662] [INSPIRE].

[18] T. Neumann and M. Wiesemann, *Finite top-mass effects in gluon-induced Higgs production with a jet-veto at NNLO*, *JHEP* **11** (2014) 150 [arXiv:1408.6836] [INSPIRE].

[19] M. Czakon, R.V. Harlander, J. Klappert and M. Niggetiedt, *Exact Top-Quark Mass Dependence in Hadronic Higgs Production*, *Phys. Rev. Lett.* **127** (2021) 162002 [arXiv:2105.04436] [INSPIRE].

[20] S. Catani, L. Cieri, D. de Florian, G. Ferrera and M. Grazzini, *Diphoton production at hadron colliders: a fully-differential QCD calculation at NNLO*, *Phys. Rev. Lett.* **108** (2012) 072001 [*Erratum ibid.* **117** (2016) 089901] [arXiv:1110.2375] [INSPIRE].

[21] J.M. Campbell, R.K. Ellis, Y. Li and C. Williams, *Predictions for diphoton production at the LHC through NNLO in QCD*, *JHEP* **07** (2016) 148 [arXiv:1603.02663] [INSPIRE].

[22] M. Grazzini, S. Kallweit, D. Rathlev and A. Torre, *$Z\gamma$ production at hadron colliders in NNLO QCD*, *Phys. Lett. B* **731** (2014) 204 [arXiv:1309.7000] [INSPIRE].

[23] M. Grazzini, S. Kallweit and D. Rathlev, *$W\gamma$ and $Z\gamma$ production at the LHC in NNLO QCD*, *JHEP* **07** (2015) 085 [arXiv:1504.01330] [INSPIRE].

[24] J.M. Campbell, T. Neumann and C. Williams, *$Z\gamma$ Production at NNLO Including Anomalous Couplings*, *JHEP* **11** (2017) 150 [arXiv:1708.02925] [INSPIRE].

[25] T. Gehrmann, N. Glover, A. Huss and J. Whitehead, *Scale and isolation sensitivity of diphoton distributions at the LHC*, *JHEP* **01** (2021) 108 [arXiv:2009.11310] [INSPIRE].

[26] F. Cascioli et al., *ZZ production at hadron colliders in NNLO QCD*, *Phys. Lett. B* **735** (2014) 311 [arXiv:1405.2219] [INSPIRE].

[27] M. Grazzini, S. Kallweit and D. Rathlev, *ZZ production at the LHC: fiducial cross sections and distributions in NNLO QCD*, *Phys. Lett. B* **750** (2015) 407 [arXiv:1507.06257] [INSPIRE].

[28] G. Heinrich, S. Jahn, S.P. Jones, M. Kerner and J. Pires, *NNLO predictions for Z-boson pair production at the LHC*, *JHEP* **03** (2018) 142 [arXiv:1710.06294] [INSPIRE].

[29] S. Kallweit and M. Wiesemann, *ZZ production at the LHC: NNLO predictions for $2\ell2\nu$ and 4ℓ signatures*, *Phys. Lett. B* **786** (2018) 382 [arXiv:1806.05941] [INSPIRE].

[30] T. Gehrmann et al., *W^+W^- Production at Hadron Colliders in Next to Next to Leading Order QCD*, *Phys. Rev. Lett.* **113** (2014) 212001 [arXiv:1408.5243] [INSPIRE].

[31] M. Grazzini, S. Kallweit, S. Pozzorini, D. Rathlev and M. Wiesemann, *W^+W^- production at the LHC: fiducial cross sections and distributions in NNLO QCD*, *JHEP* **08** (2016) 140 [arXiv:1605.02716] [INSPIRE].

[32] M. Grazzini, S. Kallweit, D. Rathlev and M. Wiesemann, *$W^{\pm}Z$ production at hadron colliders in NNLO QCD*, *Phys. Lett. B* **761** (2016) 179 [arXiv:1604.08576] [INSPIRE].

[33] M. Grazzini, S. Kallweit, D. Rathlev and M. Wiesemann, $W^\pm Z$ *production at the LHC: fiducial cross sections and distributions in NNLO QCD*, *JHEP* **05** (2017) 139 [arXiv:1703.09065] [INSPIRE].

[34] D. de Florian and J. Mazzitelli, *Higgs Boson Pair Production at Next-to-Next-to-Leading Order in QCD*, *Phys. Rev. Lett.* **111** (2013) 201801 [arXiv:1309.6594] [INSPIRE].

[35] D. de Florian et al., *Differential Higgs Boson Pair Production at Next-to-Next-to-Leading Order in QCD*, *JHEP* **09** (2016) 151 [arXiv:1606.09519] [INSPIRE].

[36] M. Grazzini et al., *Higgs boson pair production at NNLO with top quark mass effects*, *JHEP* **05** (2018) 059 [arXiv:1803.02463] [INSPIRE].

[37] J. Baglio, A. Djouadi, R. Gröber, M.M. Mühlleitner, J. Quevillon and M. Spira, *The measurement of the Higgs self-coupling at the LHC: theoretical status*, *JHEP* **04** (2013) 151 [arXiv:1212.5581] [INSPIRE].

[38] H.T. Li and J. Wang, *Fully Differential Higgs Pair Production in Association With a W Boson at Next-to-Next-to-Leading Order in QCD*, *Phys. Lett. B* **765** (2017) 265 [arXiv:1607.06382] [INSPIRE].

[39] D. de Florian, I. Fabre and J. Mazzitelli, *Triple Higgs production at hadron colliders at NNLO in QCD*, *JHEP* **03** (2020) 155 [arXiv:1912.02760] [INSPIRE].

[40] H.A. Chawdhry, M.L. Czakon, A. Mitov and R. Poncelet, *NNLO QCD corrections to three-photon production at the LHC*, *JHEP* **02** (2020) 057 [arXiv:1911.00479] [INSPIRE].

[41] S. Kallweit, V. Sotnikov and M. Wiesemann, *Triphoton production at hadron colliders in NNLO QCD*, *Phys. Lett. B* **812** (2021) 136013 [arXiv:2010.04681] [INSPIRE].

[42] M. Czakon, A. Mitov and R. Poncelet, *Next-to-Next-to-Leading Order Study of Three-Jet Production at the LHC*, *Phys. Rev. Lett.* **127** (2021) 152001 [arXiv:2106.05331] [INSPIRE].

[43] H.A. Chawdhry, M. Czakon, A. Mitov and R. Poncelet, *NNLO QCD corrections to diphoton production with an additional jet at the LHC*, *JHEP* **09** (2021) 093 [arXiv:2105.06940] [INSPIRE].

[44] O. Brein, A. Djouadi and R. Harlander, *NNLO QCD corrections to the Higgs-strahlung processes at hadron colliders*, *Phys. Lett. B* **579** (2004) 149 [hep-ph/0307206] [INSPIRE].

[45] O. Brein, R. Harlander, M. Wiesemann and T. Zirke, *Top-Quark Mediated Effects in Hadronic Higgs-Strahlung*, *Eur. Phys. J. C* **72** (2012) 1868 [arXiv:1111.0761] [INSPIRE].

[46] O. Brein, R.V. Harlander and T.J.E. Zirke, *vh@nnlo - Higgs Strahlung at hadron colliders*, *Comput. Phys. Commun.* **184** (2013) 998 [arXiv:1210.5347] [INSPIRE].

[47] G. Ferrera, M. Grazzini and F. Tramontano, *Higher-order QCD effects for associated WH production and decay at the LHC*, *JHEP* **04** (2014) 039 [arXiv:1312.1669] [INSPIRE].

[48] F. Caola, G. Luisoni, K. Melnikov and R. Röntsch, *NNLO QCD corrections to associated WH production and $H \to b\bar{b}$ decay*, *Phys. Rev. D* **97** (2018) 074022 [arXiv:1712.06954] [INSPIRE].

[49] R. Gauld, A. Gehrmann-De Ridder, E.W.N. Glover, A. Huss and I. Majer, *Associated production of a Higgs boson decaying into bottom quarks and a weak vector boson decaying leptonically at NNLO in QCD*, *JHEP* **10** (2019) 002 [arXiv:1907.05836] [INSPIRE].

[50] L. Altenkamp, S. Dittmaier, R.V. Harlander, H. Rzehak and T.J.E. Zirke, *Gluon-induced Higgs-strahlung at next-to-leading order QCD*, *JHEP* **02** (2013) 078 [arXiv:1211.5015] [INSPIRE].

[51] R.V. Harlander, A. Kulesza, V. Theeuwes and T. Zirke, *Soft gluon resummation for gluon-induced Higgs Strahlung*, *JHEP* **11** (2014) 082 [arXiv:1410.0217] [INSPIRE].

[52] A. Hasselhuhn, T. Luthe and M. Steinhauser, *On top quark mass effects to $gg \to ZH$ at NLO*, *JHEP* **01** (2017) 073 [arXiv:1611.05881] [INSPIRE].

[53] G. Wang, X. Xu, Y. Xu and L.L. Yang, *Next-to-leading order corrections for $gg \to ZH$ with top quark mass dependence*, *Phys. Lett. B* **829** (2022) 137087 [arXiv:2107.08206] [INSPIRE].

[54] J. Davies, G. Mishima and M. Steinhauser, *Virtual corrections to $gg \to ZH$ in the high-energy and large-m_t limits*, *JHEP* **03** (2021) 034 [arXiv:2011.12314] [INSPIRE].

[55] L. Chen, G. Heinrich, S.P. Jones, M. Kerner, J. Klappert and J. Schlenk, *ZH production in gluon fusion: two-loop amplitudes with full top quark mass dependence*, *JHEP* **03** (2021) 125 [arXiv:2011.12325] [INSPIRE].

[56] L. Alasfar, G. Degrassi, P.P. Giardino, R. Gröber and M. Vitti, *Virtual corrections to $gg \to ZH$ via a transverse momentum expansion*, *JHEP* **05** (2021) 168 [arXiv:2103.06225] [INSPIRE].

[57] R.V. Harlander, J. Klappert, C. Pandini and A. Papaefstathiou, *Exploiting the WH/ZH symmetry in the search for New Physics*, *Eur. Phys. J. C* **78** (2018) 760 [arXiv:1804.02299] [INSPIRE].

[58] S. Dawson, T. Han, W.K. Lai, A.K. Leibovich and I. Lewis, *Resummation Effects in Vector-Boson and Higgs Associated Production*, *Phys. Rev. D* **86** (2012) 074007 [arXiv:1207.4207] [INSPIRE].

[59] D.Y. Shao, C.S. Li and H.T. Li, *Resummation Prediction on Higgs and Vector Boson Associated Production with a Jet Veto at the LHC*, *JHEP* **02** (2014) 117 [arXiv:1309.5015] [INSPIRE].

[60] Y. Li and X. Liu, *High precision predictions for exclusive VH production at the LHC*, *JHEP* **06** (2014) 028 [arXiv:1401.2149] [INSPIRE].

[61] R. Gauld, A. Gehrmann-De Ridder, E.W.N. Glover, A. Huss and I. Majer, *Precise predictions for WH+jet production at the LHC*, *Phys. Lett. B* **817** (2021) 136335 [arXiv:2009.14209] [INSPIRE].

[62] M.L. Ciccolini, S. Dittmaier and M. Krämer, *Electroweak radiative corrections to associated WH and ZH production at hadron colliders*, *Phys. Rev. D* **68** (2003) 073003 [hep-ph/0306234] [INSPIRE].

[63] A. Denner, S. Dittmaier, S. Kallweit and A. Muck, *Electroweak corrections to Higgs-strahlung off W/Z bosons at the Tevatron and the LHC with HAWK*, *JHEP* **03** (2012) 075 [arXiv:1112.5142] [INSPIRE].

[64] A. Denner, S. Dittmaier, S. Kallweit and A. Mück, *HAWK 2.0: A Monte Carlo program for Higgs production in vector-boson fusion and Higgs strahlung at hadron colliders*, *Comput. Phys. Commun.* **195** (2015) 161 [arXiv:1412.5390] [INSPIRE].

[65] G. Luisoni, P. Nason, C. Oleari and F. Tramontano, *$HW^{\pm}/HZ + 0$ and 1 jet at NLO with the POWHEG BOX interfaced to GoSam and their merging within MiNLO*, *JHEP* **10** (2013) 083 [arXiv:1306.2542] [INSPIRE].

[66] K. Hamilton, P. Nason and G. Zanderighi, *MINLO: Multi-Scale Improved NLO*, *JHEP* **10** (2012) 155 [arXiv:1206.3572] [INSPIRE].

[67] K. Hamilton, P. Nason, C. Oleari and G. Zanderighi, *Merging H/W/Z + 0 and 1 jet at NLO with no merging scale: a path to parton shower + NNLO matching*, *JHEP* **05** (2013) 082 [arXiv:1212.4504] [INSPIRE].

[68] F. Granata, J.M. Lindert, C. Oleari and S. Pozzorini, *NLO QCD+EW predictions for HV and HV +jet production including parton-shower effects*, *JHEP* **09** (2017) 012 [arXiv:1706.03522] [INSPIRE].

[69] B. Hespel, F. Maltoni and E. Vryonidou, *Higgs and Z boson associated production via gluon fusion in the SM and the 2HDM*, *JHEP* **06** (2015) 065 [arXiv:1503.01656] [INSPIRE].

[70] D. Goncalves, F. Krauss, S. Kuttimalai and P. Maierhöfer, *Higgs-Strahlung: Merging the NLO Drell-Yan and Loop-Induced 0 + 1 jet Multiplicities*, *Phys. Rev. D* **92** (2015) 073006 [arXiv:1509.01597] [INSPIRE].

[71] S. Amoroso et al., *Les Houches 2019: Physics at TeV Colliders: Standard Model Working Group Report*, in *11th Les Houches Workshop on Physics at TeV Colliders: PhysTeV Les Houches*, (2020) [arXiv:2003.01700] [INSPIRE].

[72] K. Mimasu, V. Sanz and C. Williams, *Higher Order QCD predictions for Associated Higgs production with anomalous couplings to gauge bosons*, *JHEP* **08** (2016) 039 [arXiv:1512.02572] [INSPIRE].

[73] K. Hamilton, P. Nason, E. Re and G. Zanderighi, *NNLOPS simulation of Higgs boson production*, *JHEP* **10** (2013) 222 [arXiv:1309.0017] [INSPIRE].

[74] S. Höche, Y. Li and S. Prestel, *Drell-Yan lepton pair production at NNLO QCD with parton showers*, *Phys. Rev. D* **91** (2015) 074015 [arXiv:1405.3607] [INSPIRE].

[75] S. Höche, Y. Li and S. Prestel, *Higgs-boson production through gluon fusion at NNLO QCD with parton showers*, *Phys. Rev. D* **90** (2014) 054011 [arXiv:1407.3773] [INSPIRE].

[76] S. Alioli, C.W. Bauer, C. Berggren, F.J. Tackmann, J.R. Walsh and S. Zuberi, *Matching Fully Differential NNLO Calculations and Parton Showers*, *JHEP* **06** (2014) 089 [arXiv:1311.0286] [INSPIRE].

[77] P.F. Monni, P. Nason, E. Re, M. Wiesemann and G. Zanderighi, *MiNNLO_PS: a new method to match NNLO QCD to parton showers*, *JHEP* **05** (2020) 143 [arXiv:1908.06987] [INSPIRE].

[78] P.F. Monni, E. Re and M. Wiesemann, *MiNNLO_PS: optimizing $2 \to 1$ hadronic processes*, *Eur. Phys. J. C* **80** (2020) 1075 [arXiv:2006.04133] [INSPIRE].

[79] K. Hamilton, P. Nason and G. Zanderighi, *Finite quark-mass effects in the NNLOPS POWHEG+MiNLO Higgs generator*, *JHEP* **05** (2015) 140 [arXiv:1501.04637] [INSPIRE].

[80] A. Karlberg, E. Re and G. Zanderighi, *NNLOPS accurate Drell-Yan production*, *JHEP* **09** (2014) 134 [arXiv:1407.2940] [INSPIRE].

[81] S. Alioli, C.W. Bauer, C. Berggren, F.J. Tackmann and J.R. Walsh, *Drell-Yan production at NNLL'+NNLO matched to parton showers*, *Phys. Rev. D* **92** (2015) 094020 [arXiv:1508.01475] [INSPIRE].

[82] W. Astill, W. Bizoń, E. Re and G. Zanderighi, *NNLOPS accurate associated HZ production with $H \to b\bar{b}$ decay at NLO*, *JHEP* **11** (2018) 157 [arXiv:1804.08141] [INSPIRE].

[83] S. Alioli, A. Broggio, S. Kallweit, M.A. Lim and L. Rottoli, *Higgsstrahlung at NNLL'+NNLO matched to parton showers in GENEVA*, *Phys. Rev. D* **100** (2019) 096016 [arXiv:1909.02026] [INSPIRE].

[84] W. Astill, W. Bizon, E. Re and G. Zanderighi, *NNLOPS accurate associated HW production*, *JHEP* **06** (2016) 154 [arXiv:1603.01620] [InSPIRE].

[85] S. Alioli et al., *Precise predictions for photon pair production matched to parton showers in GENEVA*, *JHEP* **04** (2021) 041 [arXiv:2010.10498] [InSPIRE].

[86] D. Lombardi, M. Wiesemann and G. Zanderighi, *Advancing MiNNLO$_{PS}$ to diboson processes: $Z\gamma$ production at NNLO+PS*, *JHEP* **06** (2021) 095 [arXiv:2010.10478] [InSPIRE].

[87] D. Lombardi, M. Wiesemann and G. Zanderighi, *Anomalous couplings in $Z\gamma$ events at NNLO+PS and improving $\nu\bar{\nu}\gamma$ backgrounds in dark-matter searches*, *Phys. Lett. B* **824** (2022) 136846 [arXiv:2108.11315] [InSPIRE].

[88] T. Cridge, M.A. Lim and R. Nagar, *$W\gamma$ production at NNLO+PS accuracy in Geneva*, *Phys. Lett. B* **826** (2022) 136918 [arXiv:2105.13214] [InSPIRE].

[89] S. Alioli et al., *Next-to-next-to-leading order event generation for Z boson pair production matched to parton shower*, *Phys. Lett. B* **818** (2021) 136380 [arXiv:2103.01214] [InSPIRE].

[90] L. Buonocore, G. Koole, D. Lombardi, L. Rottoli, M. Wiesemann and G. Zanderighi, *ZZ production at nNNLO+PS with MiNNLO$_{PS}$*, *JHEP* **01** (2022) 072 [arXiv:2108.05337] [InSPIRE].

[91] E. Re, M. Wiesemann and G. Zanderighi, *NNLOPS accurate predictions for W^+W^- production*, *JHEP* **12** (2018) 121 [arXiv:1805.09857] [InSPIRE].

[92] D. Lombardi, M. Wiesemann and G. Zanderighi, *W^+W^- production at NNLO+PS with MINNLO$_{PS}$*, *JHEP* **11** (2021) 230 [arXiv:2103.12077] [InSPIRE].

[93] J. Mazzitelli, P.F. Monni, P. Nason, E. Re, M. Wiesemann and G. Zanderighi, *Next-to-Next-to-Leading Order Event Generation for Top-Quark Pair Production*, *Phys. Rev. Lett.* **127** (2021) 062001 [arXiv:2012.14267] [InSPIRE].

[94] S.G. Gorishnii, A.L. Kataev, S.A. Larin and L.R. Surguladze, *Three Loop QCD Correction to the Correlator of the Quark Scalar Currents and $\Gamma_{\rm tot}(H^0 \to Hadrons)$*, *Mod. Phys. Lett. A* **5** (1990) 2703 [InSPIRE].

[95] S.G. Gorishnii, A.L. Kataev, S.A. Larin and L.R. Surguladze, *Scheme dependence of the next to next-to-leading QCD corrections to $\Gamma_{\rm tot}(H^0 \to hadrons)$ and the spurious QCD infrared fixed point*, *Phys. Rev. D* **43** (1991) 1633 [InSPIRE].

[96] A.L. Kataev and V.T. Kim, *The Effects of the QCD corrections to $\Gamma(H^0 \to b\bar{b})$*, *Mod. Phys. Lett. A* **9** (1994) 1309 [InSPIRE].

[97] L.R. Surguladze, *Quark mass effects in fermionic decays of the Higgs boson in $O(\alpha_S^2)$ perturbative QCD*, *Phys. Lett. B* **341** (1994) 60 [hep-ph/9405325] [InSPIRE].

[98] S.A. Larin, T. van Ritbergen and J.A.M. Vermaseren, *The Large top quark mass expansion for Higgs boson decays into bottom quarks and into gluons*, *Phys. Lett. B* **362** (1995) 134 [hep-ph/9506465] [InSPIRE].

[99] K.G. Chetyrkin and A. Kwiatkowski, *Second order QCD corrections to scalar and pseudoscalar Higgs decays into massive bottom quarks*, *Nucl. Phys. B* **461** (1996) 3 [hep-ph/9505358] [InSPIRE].

[100] K.G. Chetyrkin, *Correlator of the quark scalar currents and $\Gamma_{\rm tot}(H \to hadrons)$ at $O(\alpha_S^3)$ in pQCD*, *Phys. Lett. B* **390** (1997) 309 [hep-ph/9608318] [InSPIRE].

[101] P.A. Baikov, K.G. Chetyrkin and J.H. Kühn, *Scalar correlator at $O(\alpha_s^4)$, Higgs decay into b-quarks and bounds on the light quark masses*, *Phys. Rev. Lett.* **96** (2006) 012003 [hep-ph/0511063] [INSPIRE].

[102] J. Davies, M. Steinhauser and D. Wellmann, *Completing the hadronic Higgs boson decay at order α_s^4*, *Nucl. Phys. B* **920** (2017) 20 [arXiv:1703.02988] [INSPIRE].

[103] J. Fleischer and F. Jegerlehner, *Radiative Corrections to Higgs Decays in the Extended Weinberg-Salam Model*, *Phys. Rev. D* **23** (1981) 2001 [INSPIRE].

[104] D.Y. Bardin, B.M. Vilensky and P.K. Khristova, *Calculation of the Higgs boson decay width into fermion pairs*, *Sov. J. Nucl. Phys.* **53** (1991) 152 [INSPIRE].

[105] A. Dabelstein and W. Hollik, *Electroweak corrections to the fermionic decay width of the standard Higgs boson*, *Z. Phys. C* **53** (1992) 507 [INSPIRE].

[106] B.A. Kniehl, *Radiative corrections for $H \to f\bar{f}(\gamma)$ in the standard model*, *Nucl. Phys. B* **376** (1992) 3 [INSPIRE].

[107] A. Denner, S. Heinemeyer, I. Puljak, D. Rebuzzi and M. Spira, *Standard Model Higgs-Boson Branching Ratios with Uncertainties*, *Eur. Phys. J. C* **71** (2011) 1753 [arXiv:1107.5909] [INSPIRE].

[108] M. Spira, *Higgs Boson Production and Decay at Hadron Colliders*, *Prog. Part. Nucl. Phys.* **95** (2017) 98 [arXiv:1612.07651] [INSPIRE].

[109] E. Braaten and J.P. Leveille, *Higgs Boson Decay and the Running Mass*, *Phys. Rev. D* **22** (1980) 715 [INSPIRE].

[110] M. Drees and K.-i. Hikasa, *Note on QCD corrections to hadronic Higgs decay*, *Phys. Lett. B* **240** (1990) 455 [*Erratum ibid.* **262** (1991) 497] [INSPIRE].

[111] N. Sakai, *Perturbative QCD Corrections to the Hadronic Decay Width of the Higgs Boson*, *Phys. Rev. D* **22** (1980) 2220 [INSPIRE].

[112] P. Janot, *First Order QED and QCD Radiative Corrections to Higgs Decay Into Massive Fermions*, *Phys. Lett. B* **223** (1989) 110 [INSPIRE].

[113] C. Anastasiou, F. Herzog and A. Lazopoulos, *The fully differential decay rate of a Higgs boson to bottom-quarks at NNLO in QCD*, *JHEP* **03** (2012) 035 [arXiv:1110.2368] [INSPIRE].

[114] V. Del Duca, C. Duhr, G. Somogyi, F. Tramontano and Z. Trócsányi, *Higgs boson decay into b-quarks at NNLO accuracy*, *JHEP* **04** (2015) 036 [arXiv:1501.07226] [INSPIRE].

[115] F. Caola, K. Melnikov and R. Röntsch, *Analytic results for decays of color singlets to gg and $q\bar{q}$ final states at NNLO QCD with the nested soft-collinear subtraction scheme*, *Eur. Phys. J. C* **79** (2019) 1013 [arXiv:1907.05398] [INSPIRE].

[116] W. Bernreuther, L. Chen and Z.-G. Si, *Differential decay rates of CP-even and CP-odd Higgs bosons to top and bottom quarks at NNLO QCD*, *JHEP* **07** (2018) 159 [arXiv:1805.06658] [INSPIRE].

[117] A. Behring and W. Bizoń, *Higgs decay into massive b-quarks at NNLO QCD in the nested soft-collinear subtraction scheme*, *JHEP* **01** (2020) 189 [arXiv:1911.11524] [INSPIRE].

[118] A. Behring, W. Bizoń, F. Caola, K. Melnikov and R. Röntsch, *Bottom quark mass effects in associated WH production with the $H \to b\bar{b}$ decay through NNLO QCD*, *Phys. Rev. D* **101** (2020) 114012 [arXiv:2003.08321] [INSPIRE].

[119] G. Somogyi and F. Tramontano, *Fully exclusive heavy quark-antiquark pair production from a colourless initial state at NNLO in QCD*, *JHEP* **11** (2020) 142 [arXiv:2007.15015] [INSPIRE].

[120] R. Mondini and C. Williams, $H \to b\bar{b}j$ *at next-to-next-to-leading order accuracy*, *JHEP* **06** (2019) 120 [arXiv:1904.08961] [INSPIRE].

[121] R. Mondini, M. Schiavi and C. Williams, N^3LO *predictions for the decay of the Higgs boson to bottom quarks*, *JHEP* **06** (2019) 079 [arXiv:1904.08960] [INSPIRE].

[122] A. Primo, G. Sasso, G. Somogyi and F. Tramontano, *Exact Top Yukawa corrections to Higgs boson decay into bottom quarks*, *Phys. Rev. D* **99** (2019) 054013 [arXiv:1812.07811] [INSPIRE].

[123] R. Mondini, U. Schubert and C. Williams, *Top-induced contributions to $H \to b\bar{b}$ and $H \to c\bar{c}$ at $\mathcal{O}(\alpha_s^3)$*, *JHEP* **12** (2020) 058 [arXiv:2006.03563] [INSPIRE].

[124] J.M. Cullen, B.D. Pecjak and D.J. Scott, *NLO corrections to $h \to b\bar{b}$ decay in SMEFT*, *JHEP* **08** (2019) 173 [arXiv:1904.06358] [INSPIRE].

[125] W. Bizoń, F. Caola, K. Melnikov and R. Röntsch, *Anomalous couplings in associated VH production with Higgs boson decay to massive b quarks at NNLO in QCD*, *Phys. Rev. D* **105** (2022) 014023 [arXiv:2106.06328] [INSPIRE].

[126] W. Bizoń, E. Re and G. Zanderighi, *NNLOPS description of the $H \to b\bar{b}$ decay with MiNLO*, *JHEP* **06** (2020) 006 [arXiv:1912.09982] [INSPIRE].

[127] S. Alioli et al., *Resummed predictions for hadronic Higgs boson decays*, *JHEP* **04** (2021) 254 [arXiv:2009.13533] [INSPIRE].

[128] Y. Hu, C. Sun, X.-M. Shen and J. Gao, *Hadronic decays of Higgs boson at NNLO matched with parton shower*, *JHEP* **08** (2021) 122 [arXiv:2101.08916] [INSPIRE].

[129] S. Alioli, P. Nason, C. Oleari and E. Re, *A general framework for implementing NLO calculations in shower Monte Carlo programs: the POWHEG BOX*, *JHEP* **06** (2010) 043 [arXiv:1002.2581] [INSPIRE].

[130] T. Ježo and P. Nason, *On the Treatment of Resonances in Next-to-Leading Order Calculations Matched to a Parton Shower*, *JHEP* **12** (2015) 065 [arXiv:1509.09071] [INSPIRE].

[131] ATLAS collaboration, *Measurement of the associated production of a Higgs boson decaying into b-quarks with a vector boson at high transverse momentum in pp collisions at $\sqrt{s} = 13$ TeV with the ATLAS detector*, *Phys. Lett. B* **816** (2021) 136204 [arXiv:2008.02508] [INSPIRE].

[132] T. Sjöstrand et al., *An introduction to PYTHIA 8.2*, *Comput. Phys. Commun.* **191** (2015) 159 [arXiv:1410.3012] [INSPIRE].

[133] P. Nason, *A New method for combining NLO QCD with shower Monte Carlo algorithms*, *JHEP* **11** (2004) 040 [hep-ph/0409146] [INSPIRE].

[134] P. Nason and G. Ridolfi, *A Positive-weight next-to-leading-order Monte Carlo for Z pair hadroproduction*, *JHEP* **08** (2006) 077 [hep-ph/0606275] [INSPIRE].

[135] S. Frixione, P. Nason and C. Oleari, *Matching NLO QCD computations with Parton Shower simulations: the POWHEG method*, *JHEP* **11** (2007) 070 [arXiv:0709.2092] [INSPIRE].

[136] J.M. Campbell, R.K. Ellis, R. Frederix, P. Nason, C. Oleari and C. Williams, *NLO Higgs Boson Production Plus One and Two Jets Using the POWHEG BOX, MadGraph4 and MCFM*, *JHEP* **07** (2012) 092 [arXiv:1202.5475] [INSPIRE].

[137] J. Alwall et al., *MadGraph/MadEvent v4: The New Web Generation*, *JHEP* **09** (2007) 028 [arXiv:0706.2334] [InSPIRE].

[138] F. Granata, *Electroweak and strong next-to-leading-order corrections to HV and HVj production at hadron colliders*, Ph.D. Thesis, Milan Bicocca U., Milan, Italy (2017).

[139] F. Cascioli, P. Maierhofer and S. Pozzorini, *Scattering Amplitudes with Open Loops*, *Phys. Rev. Lett.* **108** (2012) 111601 [arXiv:1111.5206] [InSPIRE].

[140] F. Buccioni, S. Pozzorini and M. Zoller, *On-the-fly reduction of open loops*, *Eur. Phys. J. C* **78** (2018) 70 [arXiv:1710.11452] [InSPIRE].

[141] F. Buccioni et al., *OpenLoops 2*, *Eur. Phys. J. C* **79** (2019) 866 [arXiv:1907.13071] [InSPIRE].

[142] G.P. Salam and J. Rojo, *A Higher Order Perturbative Parton Evolution Toolkit (HOPPET)*, *Comput. Phys. Commun.* **180** (2009) 120 [arXiv:0804.3755] [InSPIRE].

[143] T. Gehrmann and E. Remiddi, *Numerical evaluation of harmonic polylogarithms*, *Comput. Phys. Commun.* **141** (2001) 296 [hep-ph/0107173] [InSPIRE].

[144] J. Mazzitelli, P.F. Monni, P. Nason, E. Re, M. Wiesemann and G. Zanderighi, *Top-pair production at the LHC with MINNLO_PS*, *JHEP* **04** (2022) 079 [arXiv:2112.12135] [InSPIRE].

[145] P. Nason and C. Oleari, *Generation cuts and Born suppression in POWHEG*, arXiv:1303.3922 [InSPIRE].

[146] LHC HIGGS CROSS SECTION WORKING GROUP collaboration, *Handbook of LHC Higgs Cross Sections: 4. Deciphering the Nature of the Higgs Sector*, arXiv:1610.07922 [InSPIRE].

[147] A. Banfi, G.P. Salam and G. Zanderighi, *Infrared safe definition of jet flavor*, *Eur. Phys. J. C* **47** (2006) 113 [hep-ph/0601139] [InSPIRE].

[148] NNPDF collaboration, *Parton distributions from high-precision collider data*, *Eur. Phys. J. C* **77** (2017) 663 [arXiv:1706.00428] [InSPIRE].

[149] PARTICLE DATA GROUP collaboration, *Review of Particle Physics*, *PTEP* **2020** (2020) 083C01 [InSPIRE].

[150] P. Skands, S. Carrazza and J. Rojo, *Tuning PYTHIA 8.1: the Monash 2013 Tune*, *Eur. Phys. J. C* **74** (2014) 3024 [arXiv:1404.5630] [InSPIRE].

[151] M. Cacciari, G.P. Salam and G. Soyez, *The anti-k_t jet clustering algorithm*, *JHEP* **04** (2008) 063 [arXiv:0802.1189] [InSPIRE].

[152] R.V. Harlander, J. Klappert, S. Liebler and L. Simon, *vh@nnlo-v2: New physics in Higgs Strahlung*, *JHEP* **05** (2018) 089 [arXiv:1802.04817] [InSPIRE].

[153] S. Mrenna and P. Skands, *Automated Parton-Shower Variations in PYTHIA 8*, *Phys. Rev. D* **94** (2016) 074005 [arXiv:1605.08352] [InSPIRE].

[154] S. Catani, Y.L. Dokshitzer, M.H. Seymour and B.R. Webber, *Longitudinally invariant K_t clustering algorithms for hadron hadron collisions*, *Nucl. Phys. B* **406** (1993) 187 [InSPIRE].

[155] A. Banfi, G.P. Salam and G. Zanderighi, *Accurate QCD predictions for heavy-quark jets at the Tevatron and LHC*, *JHEP* **07** (2007) 026 [arXiv:0704.2999] [InSPIRE].

[156] G. Ridolfi, M. Ubiali and M. Zaro, *A fragmentation-based study of heavy quark production*, *JHEP* **01** (2020) 196 [arXiv:1911.01975] [InSPIRE].